Journal of the Mechanics and Physics of Solids 95 (2016) 1–24

Contents lists available at ScienceDirect

Journal of the Mechanics and Physics of Solids

journal homepage: www.elsevier.com/locate/jmps

Exterior statistics based boundary conditions for representative volume elements of elastic composites

Somnath Ghosh *,[1], Dhirendra V. Kubair [2]

Department of Civil, Mechanical and Materials Science & Engineering, Johns Hopkins University, 3400 N. Charles Street, Baltimore, MD 21218, United States

ARTICLE INFO

Article history:
Received 15 April 2016
Accepted 16 May 2016
Available online 20 May 2016

Keywords:
Heterogeneous microstructure
Statistically equivalent representative volume elements (SERVE)
Exterior statistics-based boundary conditions
Two-point correlation functions
Green's function
SVE

ABSTRACT

Statistically equivalent representative volume elements or SERVEs are representations of the microstructure that are used for micromechanical simulations to generate homogenized material constitutive responses and properties (Swaminathan et al., 2006a; Ghosh, 2011). Typically, a SERVE is generated from the parent microstructure as a statistically equivalent region, whose size is determined from the requirements of convergence of macroscopic properties. Standard boundary conditions, such as affine transformation-based displacement boundary conditions (ATDBCs), uniform traction boundary conditions (UTBCs) or periodic boundary conditions (PBCs) are conventionally applied on the SERVE boundary for micromechanical simulations. However, when the microstructure is characterized by arbitrary, nonuniform distributions of heterogeneities, these simple boundary conditions do not represent the effect of regions exterior to the SERVE. Improper boundary conditions can result in significantly larger than optimal SERVE domains, needed for converged properties. In an attempt to overcome the limitations of the conventional boundary conditions on the SERVE, this paper explores the effect of boundary conditions that incorporate the statistics of the exterior region on the SERVE of elastic composites. Using Green's function based interaction kernels, coupled with statistical functions of the microstructural characteristics like one-point and two-point correlation functions, a novel *exterior statistics-based boundary condition* or ESBC is derived for the SERVE. The advantages of the ESBC are established by comparing with results of simulations using conventional boundary conditions. Results of the SERVE simulations subjected to ESBCs are also compared with those from other popular methods like statistical volume element (SVE) and weighted statistical volume element (WSVE). The proposed ESBCs offer significant advantages over other methods in the SERVE-based analysis of heterogeneous materials.

1. Introduction

Composite materials have gained wide commercial acceptance due to their superior effective thermal and mechanical properties. These properties depend not only on properties of individual constituents but also on the local microstructural morphology like fiber volume fraction, inclusion size and shape, and spatial dispersion of fibers. Effective properties are

* Corresponding author.
E-mail address: sghosh20@jhu.edu (S. Ghosh).
[1] M. G. Callas Chair Professor.
[2] Assistant Research Professor.

http://dx.doi.org/10.1016/j.jmps.2016.05.022
0022-5096/

Nomenclature

RVE	representative volume element
SERVE	statistically equivalent representative volume element
ESBC	exterior statistics-based boundary condition
ATDBC	affine transformation-based displacement boundary condition
UTBC	uniform traction boundary condition
PBC	periodic boundary condition
SIGF	statistically informed Green's function
SVE	statistical volume elements
WSVE	weighted statistical volume element
MVE	microstructural volume element

evaluated by methods of homogenization or averaging of microscopic variables like stresses and strains, with various assumptions on the representative microstructural domain. A number of analytical models have evolved within the framework of small deformation elasticity theory (Eshelby, 1957; Benvensite, 1987; Hill, 1965; Hashin and Shtrikman, 1963; Hashin, 1983; Mura, 1987) to predict homogenized macroscale constitutive response of heterogeneous materials. Their underlying principle is the Hill–Mandel condition of homogeneity (Hill, 1965, 1967; Mandel, 1971), which states that for largely separated microscopic and macroscopic length scales, the volume-averaged strain energy is obtained as the product of the volume-averaged stresses and strains in representative microstructural domain. Hierarchical models, involving computational micromechanical analysis, have become increasingly popular for transfer of information from lower to higher scales, usually in the form of effective material properties (Böhm, 2004; Chung et al., 2000; Fish and Shek, 2000; Ghosh et al., 1995, 1996; Guedes and Kikuchi, 1991; Kouznetsova et al., 2002; Terada and Kikuchi, 2000; Ghosh, 2011; Willoughby et al., 2012). A number of hierarchical models incorporate the asymptotic homogenization theory with computational micromechanics models, based on scale-separation with assumptions of macroscopic homogeneity and microscopic periodicity. Uncoupling of governing equations at different scales is achieved through the incorporation of specific boundary conditions, e.g. uniform displacement, periodicity, etc., on the microscopic *representative volume elements* or RVEs. FE^2 multi-scale methods in Feyel and Chaboche (2000) solve micro-mechanical RVE models for every element integration point in the computational domain to obtain homogenized properties.

Determination of effective material properties necessitates the establishment of a microstructural representative volume element or RVE (Stroeven et al., 2004; Thomas et al., 2008; Heinrich et al., 2012). The concept of RVE was introduced in Hill (1963) as a microstructural subregion that is representative of the entire microstructure in an average sense. This was extended in Hashin and Shtrikman (1963), Jones (1975), and Drugan and Willis (1996) to a reference volume that is small compared to the entire body, for which the volume average of state variables such as strains, stresses, etc., may be taken to be the same as those for the entire body. The RVE can vary with the material property of interest, even for the same microstructure. A large number of studies have been conducted with unit cells as the RVE, consisting of a single heterogeneity in a regular (square, cubic, hexagonal, etc.) matrix (Zeman and Sejnoha, 2007). The underlying assumption in these studies is that the microstructure is a uniform, periodically repetitive array of heterogeneities and the body is subjected to homogeneous boundary conditions. The occurrence of perfect uniformity or periodicity is however rare for many heterogeneous microstructures, as shown in the composite microstructure of Fig. 1(a) (Shan and Gokhale, 2002). For these non-uniform microstructures it is difficult or even impossible to identify RVEs following the strict definitions. In these cases, it is important to identify *statistically equivalent RVEs* or SERVEs for meaningful simulation of microscopic regions. Methods of identifying the SERVE from morphological considerations, using a combination of statistical and computational analyses, have been proposed in Swaminathan et al. (2006a,b) and Ghosh (2011). The SERVE is identified as the smallest, statistically equivalent region of the microstructure, e.g. the micrograph in Fig. 1, that exhibits the following characteristics.

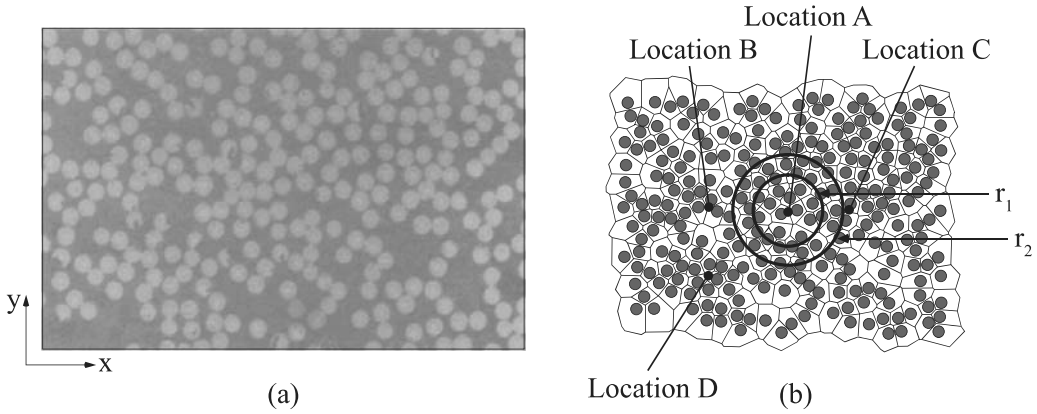

Fig. 1. (a) Optical micrograph of a fiber-reinforced composite microstructure; (b) computer simulated microstructure tessellated into Voronoi cells showing microstructural RVE regions.

1. Effective material properties of the SERVE should be equivalent to the properties of the entire microstructure, at least locally.
2. Distribution functions of parameters reflecting the local morphology in the SERVE should be equivalent to those for the overall microstructure.
3. The SERVE should be independent of location in the microstructure, as well as of the applied loading.

The second characteristic assumes that for a given property, the set of distributions functions should depend on what set of morphological parameters control that property. Fig. 1(b) shows an image of the micrograph, tessellated into a network of Voronoi cells (Ghosh, 2011). The circular region is used to identify N inclusions belonging to a SERVE. In Swaminathan et al. (2006a, b) and Ghosh (2011) the size of the SERVE is obtained by systematically increasing its simulated volume till convergence is achieved with respect to specific homogenized properties.

Various statistical descriptors have been used to estimate the size of the SERVE e.g. in Pyrz (1994), Torquato (1997), Zeman and Sejnoha (2007), Kanit et al. (2003), Al-Ostaz et al. (2007), and Romanov et al. (2013). These descriptors include distributions of the local fiber-volume-fraction, nearest-neighbor-distance, radial-basis-functions or the n-point correlation functions introduced in Jiao et al. (2007a,b) for microstructure reconstruction and homogenization. Another popular method of computational homogenization is through the use of statistical volume elements or SVEs. SVEs are typically smaller than the RVEs or SERVEs. In general, a large number of SVE instantiations are analyzed and their homogenized responses are cumulatively averaged to obtain converged properties (Yin et al., 2008; McDowell et al., 2011). However, the SVE-based methodology can sometimes converge to inaccurate values of the material properties. To overcome this limitation, a weighted SVE concept has been proposed in Qidwai et al. (2012), wherein the cumulative averages are weighted by values of statistical descriptors such as the two-point correlation functions.

In general, the RVE-based methods of property determination are concerned only with the size of the representative microstructural domain. No consideration is given to the appropriateness of the boundary conditions applied to the RVE for solving the micromechanics problem. Conventionally, three types of boundary conditions are applied on the RVEs. These are:

1. *Affine transformation-based displacement boundary condition* (*ATDBC*): This is defined as $u_i^A = \epsilon_{ij}^0 x_j$ on the RVE boundary Γ, where ϵ_{ij}^0 is a constant applied far-field strain and x_j are the boundary positions, measured from the geometrical centroid of the RVE.
2. *Uniform traction boundary condition* (*UTBC*): This is given as $T_i = \sigma_{ij}^0 n_j$ on Γ, where σ_{ij}^0 is the constant applied stress and n_j is the unit normal to the boundary of the RVE.
3. *Periodic boundary condition* (*PBCs*): This is given as $u_i^P = \epsilon_{ij}^0 x_j + u_i^{pd}$ on Γ, where the periodic additional displacement u_i^{pd} is equal on opposite faces of the RVE. This condition requires the boundary to be homologous.

Detailed studies on the effects of subjecting RVEs to uniform strain boundary condition (yielding the lower bound (Reuss)) and uniform traction boundary condition (yielding the upper bound (Voigt)) have been conducted in Hazanov and Huet (1994), Zohdi and Wriggers (2004), and Ostoja-Starzewski (2007). The underlying assumption of these boundary conditions is that strains and/or stresses in the domain exterior to the RVE are constant. They assume that the RVE is immersed in a continuum exterior to the RVE, whose strain energy density is spatially invariant and ignores the presence and interaction effects of heterogeneities exterior to the RVE. The periodic boundary condition, on the other hand, automatically repeats the microstructure, thereby rendering the deformation and damage patterns in the domain exterior to the RVE homologous. For composites with non-uniform distributions, these assumptions of strain energy invariance or periodicity are poor representations of the reality in the vicinity of the exterior RVE boundary. These boundary conditions can result in a significant over-estimation of the RVE region due to convergence requirements.

This paper is aimed at developing a novel boundary condition for the statistically equivalent RVE of SERVE, overcoming limitations of the conventionally applied boundary conditions. The interior of the SERVE should optimally encompass a microstructural region that is required to represent the essential deformation mechanisms, and the effect of its exterior domain should be imposed through realistic boundary conditions. This paper formulates a realistic boundary condition for the SERVE, based on the statistics of the exterior microstructure. The material considered is a nonuniformly dispersed fiber-reinforced elastic composite. Section 2 describes a method of reduction from the large microstructural problem to the modified SERVE problem. The exterior statistics-based boundary conditions (ESBC) are developed in Section 3 and their implementation is discussed in Section 4. Validation tests of the SERVE with ESBCs are conducted in Section 5. In Section 6, the SERVE with ESBC is compared with emerging methods of homogenization, viz. those with statistical volume elements (SVE) and weighted statistical volume elements (WSVE). The paper concludes with a summary of the novelty of this method in Section 7. Various terms and definitions are given in the nomenclature section.

2. Reduction from microstructural to modified SERVE boundary value problem

Homogenized macroscopic material properties, derived from the SERVE, should be equivalent to those for the entire microstructure such as the micrograph of Fig. 1(a). This microscopic domain, underlying a single macroscopic point, is

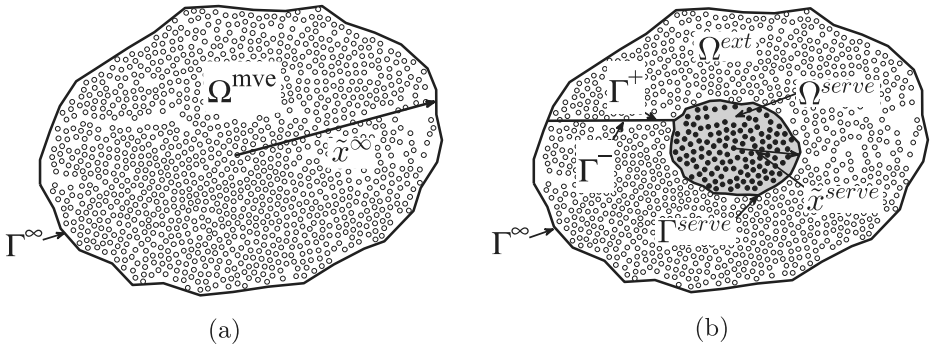

Fig. 2. Schematic view of: (a) the microstructural domain MVE Ω^{mve} and (b) the MVE containing the SERVE along with the exterior domain, i.e. $\Omega^{mve} = \Omega^{ext} \cup \Omega^{serve}$.

designated as the microstructural volume element or MVE occupying a locally infinite region $\Omega^{mve} \to \Omega^{\infty}$ as shown in Fig. 2 (a). The MVE boundary is designated as Γ^{∞} that corresponds to the boundary of an infinite domain. The MVE is assumed to consist of nonuniformly dispersed heterogeneities, e.g. fibers, particulates, etc.

The spatially invariant, volume-averaged or homogenized stresses $\bar{\sigma}_{ij}^{mve}$ and strains $\bar{\epsilon}_{ij}^{mve}$ for the MVE are expressed as:

$$\bar{\sigma}_{ij}^{mve} = \frac{1}{\Omega^{mve}} \int_{\Omega^{mve}} \sigma_{ij}^{mve}(\mathbf{x}) d\Omega \quad \text{and} \quad \bar{\epsilon}_{ij}^{mve} = \frac{1}{\Omega^{mve}} \int_{\Omega^{mve}} \epsilon_{ij}^{mve}(\mathbf{x}) d\Omega \tag{1}$$

where $\sigma_{ij}^{mve}\left(\mathbf{x}\right)$ and $\epsilon_{ij}^{mve}\left(\mathbf{x}\right)$ are respectively the spatially varying microscopic stresses and strains in the MVE. The homogenized stresses and strains for a linear elastic material are related as:

$$\bar{\sigma}_{ij}^{mve} = \bar{C}_{ijkl}^{mve} \bar{\epsilon}_{kl}^{mve} \tag{2}$$

where $\bar{C}_{ijkl}^{mve}$ is the homogenized stiffness tensor of the MVE. This stiffness can be obtained by solving a boundary value problem using the finite element method, resulting from the minimization of the total potential energy of the MVE, subject to an applied macroscopic strain field ϵ_{ij}^{0}. The corresponding principle of virtual work and the associated affine-displacement boundary conditions on Γ^{∞} are written as:

$$\int_{\Omega^{mve}} \sigma_{ij}^{mve}(\mathbf{x}) \delta\epsilon_{ij}^{mve}(\mathbf{x}) d\Omega = 0$$

subject to the affine transformation based displacement

$$u_i^A(\mathbf{x}^{\infty}) = \epsilon_{ij}^{0} x_j^{\infty} \quad \text{on } \Gamma^{\infty} \tag{3}$$

where x_j^{∞} are the coordinates of a point on the boundary Γ^{∞}, relative to a reference point such as the centroid of Ω^{mve}. The affine transformation-based applied displacements $u_i^A(\mathbf{x}^{\infty})$ on Γ^{∞} requires that the homogenized strain in the MVE be equal to the applied strain, i.e. $\bar{\epsilon}_{ij}^{mve} = \epsilon_{ij}^{0}$. To prove this, the homogenized strain is expressed as:

$$\bar{\epsilon}_{ij}^{mve} = \frac{1}{2\Omega^{mve}} \int_{\Omega^{mve}} \left(u_{i,j}^{mve}\left(\mathbf{x}\right) + u_{j,j}^{mve}\left(\mathbf{x}\right) \right) d\Omega = \frac{1}{2\Omega^{mve}} \int_{\Gamma^{\infty}} \left(u_i(\mathbf{x}) n_j(\mathbf{x}) + u_j(\mathbf{x}) n_i(\mathbf{x}) \right) d\Gamma \tag{4}$$

Expressing the displacement u_i on Γ^{∞} as $u_i^A(\mathbf{x}^{\infty}) = \epsilon_{ik}^{0} x_k$, Eq. (4) yields:

$$\bar{\epsilon}_{ij}^{mve} = \epsilon_{ik}^{0} \frac{1}{\Omega^{mve}} \int_{\Gamma^{\infty}} x_k n_j(\mathbf{x}) d\Gamma = \epsilon_{ik}^{0} \delta_{kj} = \epsilon_{ij}^{0} \tag{5}$$

This reduces Eq. (2) to

$$\bar{\sigma}_{ij}^{mve} = \bar{C}_{ijkl}^{mve} \epsilon_{kl}^{0} \tag{6}$$

Detailed micromechanical analyses of the entire MVE, to determine the $\sigma_{ij}^{mve}(\mathbf{x})$ and $\epsilon_{ij}^{mve}(\mathbf{x})$ fields, are computationally prohibitive. Hence, only a subset with explicit representation of dispersed heterogeneities, e.g. fibers, particulates, should be identified as the SERVE for detailed micromechanical analyses. This domain should be optimally small to make it computationally tractable. The ratio of the length scales of the MVE, L^{mve}, to that of the SERVE, L^{serve}, should be sufficiently large, i.e. $\frac{L^{mve}}{L^{serve}} \gg 1$.

2.1. Conventional methods of SERVE-based homogenized stiffness evaluation

Conventional computational homogenization methods perform detailed numerical analyses of the SERVE to obtain the homogenized stiffness $\bar{C}_{ijkl}^{serve}$. The finite element framework involves the principle of virtual work, together with affine

transformation-based displacement boundary conditions, stated as:

$$\int_{\Omega^{serve}} \sigma_{ij}^{serve}(\mathbf{x})\delta\epsilon_{ij}^{serve}(\mathbf{x})d\Omega = 0$$
$$\text{subjected to } u_i^A(\mathbf{x}^{serve}) = \epsilon_{ij}^0 x_j^{serve} \quad \text{on } \Gamma^{serve} \tag{7}$$

The SERVE is subjected to an applied macroscopic strain field ϵ_{ij}^0. The homogenized stresses and strains over the SERVE are expressed as:

$$\bar{\sigma}_{ij}^{serve} = \frac{1}{\Omega^{serve}}\int_{\Omega^{serve}} \sigma_{ij}(\mathbf{x})d\Omega \quad \text{and} \quad \bar{\epsilon}_{ij}^{serve} = \frac{1}{\Omega^{serve}}\int_{\Omega^{serve}} \epsilon_{ij}(\mathbf{x})d\Omega \tag{8}$$

from which the homogenized stiffness is evaluated from the relation

$$\bar{\sigma}_{ij}^{serve} = \bar{C}_{ijkl}^{serve}\bar{\epsilon}_{kl}^{serve} = \bar{C}_{ijkl}^{serve}\epsilon_{kl}^0 \tag{9}$$

The implicit assumption is that $\bar{\epsilon}_{ij}^{serve} = \epsilon_{ij}^0$ for the affine transformation-based displacements u_i^A on Γ^{serve} to hold. Comparing Eqs. (6) and (9), it is clear that the SERVE-based stiffness $\bar{C}_{ijkl}^{serve}$ can accurately represent the MVE-based stiffness $\bar{C}_{ijkl}^{mve}$, only if $\bar{\sigma}_{ij}^{serve} = \bar{\sigma}_{ij}^{mve}$. While the latter equality may hold for a few selected cases, e.g. for uniform or self-similar microstructures, it is rarely true for the general cases of arbitrarily dispersed microstructures. A novel method that can compensate for the smaller solution domain in the SERVE is therefore necessary to provide accurate homogenized material properties.

2.2. SERVE with enhanced boundary conditions for accurate stiffness evaluation

Consider that the MVE domain Ω^{mve} in Fig. 2(b) is partitioned into two complementary domains, viz. (i) the SERVE domain Ω^{serve} and (ii) a domain Ω^{ext} exterior to it, so that $\Omega^{mve} = \Omega^{ext} \cup \Omega^{serve}$. To reduce the MVE boundary value problem to that of the SERVE, the effect of the exterior domain Ω^{ext} should be manifested through equivalent conditions on the SERVE boundary Γ^{serve}. These conditions should effectively result in the same invariant strain energy for the SERVE as for the entire MVE with the applied affine displacement conditions on Γ^{∞}. The boundary conditions on Γ^{serve} should adequately reflect the interaction of Ω^{ext} with the interior Ω^{serve}.

To reduce the MVE boundary value problem in Eq. (3) to the SERVE boundary value problem, the equation of principle of virtual work is divided over the complementary domains in Fig. 2(b) as:

$$\int_{\Omega^{ext}} \sigma_{ij}^{ext}(\mathbf{x})\delta\epsilon_{ij}^{ext}(\mathbf{x})d\Omega + \int_{\Omega^{serve}} \sigma_{ij}^{serve}(\mathbf{x})\delta\epsilon_{ij}^{serve}(\mathbf{x})d\Omega = 0 \tag{10}$$

As shown in Fig. 2(b), the boundary of the exterior domain Ω^{ext} is constituted of four parts, viz. $\Gamma^{ext} = \Gamma^{\infty} \cup \Gamma^{+} \cup \Gamma^{-} \cup \Gamma^{serve}$ as shown . Here the segments Γ^{+} and Γ^{-} correspond to opposite directions of a branch cut joining Γ^{∞} and Γ^{serve}. Applying the divergence theorem to the first term containing the integral over Ω^{ext} and incorporating the stress field equilibrium conditions in the absence of body forces $\sigma_{ij,j}(\mathbf{x}) = 0$, the first term in Eq. (10) reduces to:

$$\int_{\Omega^{ext}} \sigma_{ij}^{ext}(\mathbf{x})\delta\epsilon_{ij}^{ext}(\mathbf{x})d\Omega = \int_{\Gamma^{\infty}} T_i^{ext}(\mathbf{x})\delta u_i^{ext}(\mathbf{x})d\Gamma + \int_{\Gamma^{+}} T_i^{ext}(\mathbf{x})\delta u_i^{ext}(\mathbf{x})d\Gamma - \int_{\Gamma^{-}} T_i^{ext}(\mathbf{x})\delta u_i^{ext}(\mathbf{x})d\Gamma - \int_{\Gamma^{serve}} T_i^{ext}(\mathbf{x})\delta u_i^{ext}(\mathbf{x})d\Gamma \tag{11}$$

where $T_i^{ext}(\mathbf{x}) = \sigma_{ij}^{ext}(\mathbf{x})n_j(\mathbf{x})$ is the traction component, $n_j(\mathbf{x})$ is the unit outward normal to the different boundary segments Γ and $u_i^{ext}(\mathbf{x})$ corresponds to the displacement field for the exterior domain Ω^{ext}. The second and third terms on the RHS of Eq. (11), corresponding to the boundaries Γ^{+} and Γ^{-}, are equal and opposite, and hence cancel each other.

Substituting Eq. (11) in Eq. (10), it is rewritten as:

$$\int_{\Gamma^{\infty}} T_i^{ext}(\mathbf{x})\delta u_i^{ext}(\mathbf{x})d\Gamma - \int_{\Gamma^{serve}} T_i^{ext}(\mathbf{x})\delta u_i^{ext}(\mathbf{x})d\Gamma + \int_{\Omega^{serve}} \sigma_{ij}^{serve}(\mathbf{x})\delta\epsilon_{ij}^{serve}(\mathbf{x})d\Omega = 0 \tag{12}$$

Evaluation of the homogenized stiffness $\bar{C}_{ijkl}^{mve}$ requires the solution of the boundary value problem for Ω^{mve} subject to a uniform macroscopic strain ϵ_{ij}^0. This can be realized as an applied affine transformation-based displacement $u_i^A(\mathbf{x}^{\infty}) = \epsilon_{ij}^0 x_j^{\infty}$ on Γ^{∞}. Consequently, the virtual displacement on Γ^{∞}, i.e. $\delta u_i^{ext} = 0$, which causes the first term in Eq. (12) to drop out. The principal virtual work equation thus reduces to

$$\int_{\Omega^{serve}} \sigma_{ij}^{serve}(\mathbf{x})\delta\epsilon_{ij}^{serve}(\mathbf{x})d\Omega - \int_{\Gamma^{serve}} T_i^{ext}(\mathbf{x})\delta u_i^{ext}(\mathbf{x})d\Gamma = 0 \tag{13}$$

Boundary conditions associated with Eq. (13) should be appropriately determined to represent the effect of stresses and strains in Ω^{ext} on Γ^{serve}. If displacement boundary conditions can be constructed for Γ^{serve}, then the second term on the RHS of the equation will drop out since $\delta u_i^{ext} = 0$ on Γ^{serve}.

As discussed earlier, evaluation of the homogenized stiffnesses requires the application of a macroscopic strain field $\bar{\epsilon}_{il}^{mve} = \epsilon_{il}^0$ over the MVE ($\Omega^{mve} = \Omega^{ext} \cup \Omega^{serve}$). In solving Eq. (13), the effects of Ω^{ext} and Ω^{serve} should be considered

respectively, to provide boundary conditions for Γ^{serve}. The effect of the applied strain in Ω^{serve} is manifested through the affine-transformation based boundary displacement field $u_i^A(\mathbf{x}^{serve})$ given in Eq. (7). However, the effect of the applied strain in Ω^{ext} on Γ^{serve} must also be included to accounting for microstructural non-homogeneity in this domain. This constitutes the exterior statistics-based boundary conditions for Eq. (13), written as

$$u_i^{ESBC}(\mathbf{x}^{serve}) = u_i^A(\mathbf{x}^{serve}) + u_i^{*ext}(\mathbf{x}^{serve}) \quad \text{on } \Gamma^{serve} \tag{14}$$

where u_i^{*ext} is an enhancement due to the interaction of the nonuniform exterior domain with the SERVE. In the next section, the form for u_i^{ESBC} is investigated for microstructures with nonuniform phase distributions.

3. Exterior statistics-based SERVE boundary conditions

3.1. Statistical descriptors for representing dispersed microstructures

Morphological statistics of the arbitrarily dispersed heterogeneities (fibers in this paper) in the exterior domain have a dominant effect on the traction and displacements fields on the SERVE boundary. Various statistical descriptors, such as distributions of the volume or area-fraction, nearest-neighbor-distance, etc., can be used to characterize the microstructural morphology of non-uniformly dispersed composites. The $n-point$ correlation functions have been proposed for characterization of multivariate point sets in Torquato (1997) and Jiao et al. (2007a) and can be used to effectively describe arbitrary distributions in composites.

Let $\iota^M(\mathbf{x})$ and $\iota^{F_I}(\mathbf{x})$ denote location-dependent indicator functions defined as:

$$\iota^M(\mathbf{x}) = \begin{cases} 1 & \forall\, \mathbf{x} \in \Omega^M \\ 0 & \forall\, \mathbf{x} \notin \Omega^M \end{cases} \quad \text{and} \quad \iota^{F_I}(\mathbf{x}) = \begin{cases} 1 & \forall\, \mathbf{x} \in \Omega^{F_I} \\ 0 & \forall\, \mathbf{x} \notin \Omega^{F_I} \end{cases} \quad I = 1 \cdots n_p \tag{15}$$

where the superscripts M and F_I correspond to the matrix- and Ith fiber-phase respectively, and n_p is the number of fibers. Using these indicator functions, the one-point (S_1) and two-point (S_2) correlation functions for the microstructure Ω^{mve} can be defined as:

$$S_1 = \frac{1}{\Omega^{mve}} \int_{\Omega^{mve}} \iota^F(\mathbf{x}) d\Omega \tag{16}$$

$$S_2(\mathbf{r}) = \frac{1}{\Omega^{mve}} \int_{\Omega^{mve}} \iota^F(\mathbf{x}) \iota^F(\mathbf{x} + \mathbf{r}) d\Omega \tag{17}$$

where $\mathbf{r} = (r, \theta)$ is the position vector separating two points in the domain, with $r = |\mathbf{r}|$ corresponding to the separation distance and $\theta = \angle \mathbf{r}$ is the orientation of the line joining these points with a reference direction. In composites containing equi-radius fibers, the centroids can represent these points. The one-point correlation function corresponds to the fiber volume fraction i.e. $S_1 = \Phi$ for the entire domain. For multi-phase microstructures, the two-point correlation function S_2 is defined as the probability that two points at positions $\mathbf{x}^i$ and $\mathbf{x}^j$ and separated by a distance r^{ij} at an orientation θ^{ij} lie in the same phase α. The function S_2 is able to characterize anisotropy due to its dependence on the orientation. It reduces to the radial distribution function, which is only a function of r^{ij} for isotropic distributions. It has been discussed in Torquato (2002) that the spatial statistics of a two-phase medium can be completely described by specifying the volume fraction and two-point correlation functions $S_2(r, \theta)$. Hence, in this work, these are used as the characteristic distribution functions representing microstructural morphology.

3.2. Reduction to an eigenstrain-based matrix problem

The presence of inclusions or fibers alters the spatially invariant, homogeneous state of the matrix stress σ_{ij}^M, strain ϵ_{ij}^M and displacement u_i^M fields in the MVE domain Ω^{mve}. The perturbed stress σ_{ij}^*, strain ϵ_{ij}^* and displacement u_i^* fields depend on the morphological characteristics of the microstructure, e.g. inclusion/fiber geometry and location. The total stress σ_{ij}, strain ϵ_{ij} and displacement u_i fields in the heterogeneous MVE domain may be defined as the sum of the homogeneous and perturbed parts as:

$$\sigma_{ij}(\mathbf{x}) = \sigma_{ij}^M + \sigma_{ij}^*(\mathbf{x}),\ \epsilon_{ij}(\mathbf{x}) = \epsilon_{ij}^M + \epsilon_{ij}^*(\mathbf{x}), \quad \text{and} \quad u_i(\mathbf{x}) = u_i^M + u_i^*(\mathbf{x}) \tag{18}$$

For elastic constituent phases, the total stress at a point in the MVE is defined as:

$$\sigma_{ij}(\mathbf{x}) = C_{ijkl}(\mathbf{x})\epsilon_{kl}(\mathbf{x}) = C_{ijkl}^M \epsilon_{kl}^M + \sigma_{ij}^*(\mathbf{x}) \tag{19}$$

where the location-dependent elastic stiffness tensor is written, using indicator functions, as:

$$C_{ijkl}(\mathbf{x}) = \iota^M(\mathbf{x}) C_{ijkl}^M + \iota^{F_I}(\mathbf{x}) C_{ijkl}^{F_I} \quad \forall\, I = 1 \cdots n_p \tag{20}$$

Using Eqs. (20), (19), and (18), the perturbed stress may be related to the perturbed strain as:

$$\sigma_{ij}^{*}(\mathbf{x}) = \Big(\Big[\imath^{M}(\mathbf{x}) C_{ijkl}^{M} + \imath^{F_I}(\mathbf{x}) C_{ijkl}^{F_I} \Big] - C_{ijkl}^{M} \Big) \epsilon_{kl}^{M} + \Big(\imath^{M}(\mathbf{x}) C_{ijkl}^{M} + \imath^{F_I}(\mathbf{x}) C_{ijkl}^{F_I} \Big) \epsilon_{kl}^{*}(\mathbf{x}) \tag{21}$$

which implies:

$$\begin{aligned} \sigma_{ij}^{*}(\mathbf{x}^{M}) &= C_{ijkl}^{M} \epsilon_{kl}^{*}(\mathbf{x}^{M}) \ \forall \ \{\mathbf{x}^{M} | \mathbf{x} \in \Omega^{M}\} \text{: (Matrix } M\text{)} \\ \sigma_{ij}^{*}(\mathbf{x}^{F_I}) &= \Big(C_{ijkl}^{F_I} - C_{ijkl}^{M} \Big) \epsilon_{kl}^{M} + C_{ijkl}^{F_I} \epsilon_{kl}^{*}(\mathbf{x}^{F_I}) \ \forall \ \{\mathbf{x}^{F_I} | \mathbf{x} \in \Omega^{F_I}\} \text{: (Fiber } F_I\text{)} \end{aligned} \tag{22}$$

where Ω^{M} and Ω^{F_I} correspond to the domains of the matrix and the inclusion F_I respectively. The kinematic relations for the perturbed strains and displacements are expressed as:

$$\epsilon_{ij}^{*}(\mathbf{x}) = \frac{1}{2} \Big(u_{i,j}^{*}(\mathbf{x}) + u_{j,i}^{*}(\mathbf{x}) \Big) \tag{23}$$

Since the homogeneous stress σ_{ij}^{M} is divergence-free, the stress equilibrium condition for the perturbed stress fields in the absence of body forces can be written as:

$$\sigma_{ij,j}^{*}(\mathbf{x}) = 0 \tag{24}$$

Substituting Eq. (21) into Eq. (24), the governing equation for the perturbed stresses is written as:

$$\imath^{M}(\mathbf{x}) C_{ijkl}^{M} \epsilon_{kl,j}^{*}(\mathbf{x}) + \imath^{F_I}(\mathbf{x}) C_{ijkl}^{F_I} \epsilon_{kl,j}^{*}(\mathbf{x}) = 0 \tag{25}$$

The solution process to this problem of a heterogeneous medium can be simplified by introducing an eigenstrain-based equivalent inclusion approach. In this approach, an eigenstrain $\epsilon_{ij}^{\Lambda}(\mathbf{x})$ is introduced in the inclusion/fiber domain to account for a constraint the matrix imposes on the inclusions from autonomous deformation. Correspondingly, the second of Eqs. (22) for the inclusion reduces to:

$$\sigma_{ij}^{*}(\mathbf{x}^{F_I}) = C_{ijkl}^{M} \Big(\epsilon_{kl}^{*}(\mathbf{x}) + \imath^{F_I}(\mathbf{x}) \epsilon_{kl}^{\Lambda}(\mathbf{x}) \Big) \tag{26}$$

The RHS corresponds to perturbed stresses in Ω^{F_I}, in terms of the matrix stiffness. Substituting Eqs. (23) and (26), the governing equation (25) for dispersed inclusions is reduced to a differential equation of perturbed displacements in an equivalent homogeneous matrix problem with arbitrarily distributed eigenstrains, written as:

$$C_{ijkl}^{M} u_{k,lj}^{*}(\mathbf{x}) = -\imath^{F_I}(\mathbf{x}) \Big(C_{ijkl}^{M} \epsilon_{kl}^{\Lambda}(\mathbf{x}) \Big)_{,j} \tag{27}$$

The eigenstrains depend on the shape and size of the inclusion, as well as on its material property-dependent interactions with other inclusions in the ensemble.

Assuming that the eigenstrain terms $\epsilon_{kl}^{\Lambda}(\mathbf{x}^{F_I})$ in Eq. (27) represent the effect of distributed point forces on the solution $u_i^{*}(\mathbf{x})$, an infinite-space Green's function solution $G_{ij}(\mathbf{x}, \mathbf{x}^{F_I})$ is sought. The coordinates $\mathbf{x}^{F_I}$ represent the location of any point source in Ω_I^{F} for the eigenstrains. The corresponding Green's function should satisfy the differential equation:

$$C_{ijkl}^{M} G_{im,lj}(\mathbf{x}, \mathbf{x}^{F_I}) = -\delta_{km} \delta \Big(\mathbf{x} - \mathbf{x}^{F_I} \Big) \tag{28}$$

where $\delta(\mathbf{x})$ is the Dirac delta function and δ_{km} is the Kronecker delta. The perturbed displacement field in a large MVE domain with n_p dispersed fibers can be derived as a summed integral by substituting Eq. (28) into Eq. (27) as:

$$u_i^{*}(\mathbf{x}) = \sum_{I=1}^{n_p} \int_{\Omega^{F_I}} C_{klmn}^{M} G_{ik,l}(\mathbf{x}, \mathbf{x}^{F_I}) \epsilon_{mn}^{\Lambda}(\mathbf{x}^{F_I}) d\Omega \tag{29}$$

Substituting Eq. (29) in Eq. (23), the perturbed strains can be expressed in terms of eigenstrains as:

$$\epsilon_{ij}^{*}(\mathbf{x}) = \frac{1}{2} \sum_{I=1}^{n_p} \int_{\Omega^{F_I}} C_{klmn}^{M} (G_{ik,lj}(\mathbf{x}, \mathbf{x}^{F_I}) + G_{jk,li}(\mathbf{x}, \mathbf{x}^{F_I})) \epsilon_{mn}^{\Lambda}(\mathbf{x}^{F_I}) d\Omega \tag{30}$$

The solution to Eq. (29) requires Green's functions and eigenstrains $\epsilon_{mn}^{\Lambda}(\mathbf{x}^{F_I})$. For isotropic, linear elastic matrix materials, Green's function has been derived in Mura (1987) as:

$$G_{ij}(\mathbf{x}, \mathbf{x}^{F_I}) = \frac{1}{4\pi\mu} \left[\frac{\delta_{ij}}{r^{I}} - \frac{1}{4(1-\nu)} r_{,ij}^{I} \right] \tag{31}$$

where $r^{I} = |\mathbf{x} - \mathbf{x}^{F_I}|$ is the separation distance between the a source point $\mathbf{x}^{F_I}$ and a generic field point $\mathbf{x}$. The solution procedure requires eigenstrains $\epsilon_{kl}^{\Lambda}(\mathbf{x})$ for the perturbed fields due to nonuniformly dispersed and interacting fibers.

3.3. Perturbed strains and displacements with Eshelby tensors

Eigenstrains have been shown to be invariant inside ellipsoidal inclusions (Eshelby, 1957), where closed form expressions for the integrals in Eqs. (29) and (30) have been derived using elliptic integrals. A continuous function representing the distribution of eigenstrains in the MVE can be expressed by a transformation of the constant eigenstrains in each inclusion F_I, using the position-dependent indicator-functions, as:

$$\epsilon^{\Lambda}_{kl}(\mathbf{x}|\mathbf{x}\in\Omega^{mve}) = \iota^{F_I}(\mathbf{x})\epsilon^{\Lambda_{F_I}}_{kl}, \quad I = 1\cdots n_p \tag{32}$$

where $\epsilon^{\Lambda_{F_I}}_{ij} = 0 \in \Omega^{mve}\backslash\Omega^{F_I}$. Closed form solutions of Eq. (30) have been derived as:

$$\epsilon^{*}_{ij}(\mathbf{x}) = \begin{Bmatrix} S^{F_I}_{ijkl}\epsilon^{\Lambda_{F_I}}_{kl} & \forall\ \mathbf{x}\in\Omega^{F_I} \\ \hat{G}^{F_I}_{ijkl}(\mathbf{x},\mathbf{x}^I)\epsilon^{\Lambda_{F_I}}_{kl} & \forall\ \mathbf{x}\notin\Omega^{F_I} \text{ and } \mathbf{x}^I\in\Omega^{F_I} \end{Bmatrix} \quad \forall\ I = 1\cdots n_p \tag{33}$$

The position-independent, fourth order interior Eshelby tensor $S^{F_I}_{ijkl}$ for the inclusion domain Ω^{F_I} is obtained by integrating Eq. (30) for field points $\mathbf{x}^{F_I}$ in the inclusion. On the other hand, the exterior two-point Eshelby tensor $\hat{\hat{G}}^{F_I}_{ijkl}(\mathbf{x},\mathbf{x}^I)$ evolves from integration of Eq. (30) for all field points $\mathbf{x}$ exterior to Ω^{F_I} with a reference point (centroid) at $\mathbf{x}^I$. Thus interior and exterior Eshelby tensors are defined over complementary domains as:

$$S_{ijkl}(\mathbf{x}) = \begin{Bmatrix} S^{F_I}_{ijkl} & \forall\ \mathbf{x}\in\Omega^{F_I}, \\ 0 & \forall\ \mathbf{x}\in\Omega^{mve}\backslash\Omega^{F_I} \end{Bmatrix} \quad \text{and}$$
$$\hat{G}_{ijkl}(\mathbf{x},\mathbf{x}^I) = \begin{Bmatrix} 0 & \forall\ \mathbf{x}\in\Omega^{F_I} \\ \hat{\hat{G}}^{F_I}_{ijkl}(\mathbf{x},\mathbf{x}^I) & \forall\ \mathbf{x}\in\Omega^{mve}\backslash\Omega^{F_I} \end{Bmatrix} \quad I = 1\cdots n_p \tag{34}$$

Using this complementarity, a unified 2-point tensor may be defined to represent both the interior and exterior Eshelby tensors for the inclusion F_I as:

$$H_{ijkl}(\mathbf{x},\hat{\mathbf{x}}) = \iota^{F_I}(\mathbf{x})S^{F_I}_{ijkl} + (1-\iota^{F_I}(\mathbf{x}))\hat{\hat{G}}^{F_I}_{ijkl}(\mathbf{x},\hat{\mathbf{x}}) \quad \forall\ \mathbf{x}\in\Omega^{mve} \tag{35}$$

and where $\hat{\mathbf{x}}$ is a reference point in the inclusion F_I. For a cylindrical fiber of circular cross-section with a radius a and centroid at $\mathbf{x}^I$, the interior and exterior Eshelby tensors S_{ijkl} and $\hat{\hat{G}}_{ijkl}(\mathbf{x},\mathbf{x}^I)$, respectively, are given in Mura (1987) as:

$$S_{ijkl} = \{\alpha\}^T\{\Theta_{ijkl}\}(\theta) \quad \text{and} \quad \hat{\hat{G}}_{ijkl}(\mathbf{x},\mathbf{x}^I) = \{\beta\}^T(r)\{\Theta_{ijkl}\}(\theta) \tag{36}$$

The material-dependent vectors $\{\alpha\}$ and $\{\beta\}$ are:

$$\{\alpha\} = \frac{1}{8\left(1-\nu^M\right)}\begin{Bmatrix} 4\nu^M-1 \\ 3-4\nu^M \\ 0 \\ 0 \\ 0 \end{Bmatrix}, \quad \{\beta\}(r) = \frac{\rho^2}{8\left(1-\nu^M\right)}\begin{Bmatrix} -2\left(1+2\nu^M\right)+9\rho^2 \\ 2-3\rho^2 \\ 4(1+2\nu^M)-12\rho^2 \\ 4-12\rho^2 \\ 16-24\rho^2 \end{Bmatrix}$$

Here $\rho = \frac{a}{r}$ with $r = |\mathbf{x}-\mathbf{x}^I|$ and $\theta = \angle(\mathbf{x}-\mathbf{x}^I)$, $\mathbf{x}$ being a generic field point. The parameter ν^M is Poisson's ratio of the matrix material. The circumference basis tensor is given as:

$$\{\Theta_{ijkl}\}(\theta) = \begin{Bmatrix} \delta_{ij}\delta_{kl} \\ \delta_{ik}\delta_{jl}+\delta_{il}\delta_{jk} \\ \delta_{ij}n_kn_l \\ n_in_j\delta_{kl} \\ n_in_jn_kn_l \end{Bmatrix}, \quad \text{where} \begin{Bmatrix} n_1 \\ n_2 \\ n_3 \end{Bmatrix} = \begin{Bmatrix} \cos\theta \\ \sin\theta \\ 1 \end{Bmatrix}$$

The perturbed strains due to any isolated (non-interacting) inclusion F_I in the MVE can be expressed by substituting Eqs. (32) and (35) in (33), as:

$$\epsilon^{*}_{ij}(\mathbf{x}) = \int_{\Omega^{mve}} H_{ijkl}(\mathbf{x},\hat{\mathbf{x}})\epsilon^{\Lambda}_{kl}(\hat{\mathbf{x}})d\hat{\mathbf{x}} \tag{37}$$

where $\hat{\mathbf{x}}$ is a point in the inclusion. The corresponding perturbed displacements may be written in terms of the Eshelby tensors as:

$$u_i^*(\mathbf{x}) = \int_{\Omega^{mve}} L_{ikl}(\mathbf{x}, \hat{\mathbf{x}})\epsilon_{kl}^{\Lambda}(\hat{\mathbf{x}})d\hat{\mathbf{x}} \tag{38}$$

where

$$L_{ikl}(\mathbf{x}, \hat{\mathbf{x}}) = \imath^{F_I}(\mathbf{x})T_{ikl}^{F_I}(\mathbf{x}, \hat{\mathbf{x}}) + \left(1 - \imath^{F_I}(\mathbf{x})\right)D_{ikl}^{F_I}(\mathbf{x}, \hat{\mathbf{x}}) \tag{39}$$

$T_{ikl}^{F_I}$ and $D_{ikl}^{F_I}$ are obtained by integrating Eq. (29) for field points in the interior and exterior domains of the inclusion F_I. For the cylindrical fiber of circular cross-section in Eq. (36), the displacement-transfer tensor in Eq. (39) is obtained as:

$$T_{ijk}(\mathbf{x}, \mathbf{x}^I) = \{\eta\}^T(r)\{\Psi_{ijk}\}(\theta) \quad \text{and} \quad D_{ijk}(\mathbf{x}, \mathbf{x}^I) = \{\gamma\}^T(r)\{\Psi_{ijk}\}(\theta) \tag{40}$$

where

$$\{\eta\}(r) = a\frac{\rho}{8(1-\nu^M)}\begin{Bmatrix} 4\nu^M - 1 \\ 3 - 4\nu^M \\ 0 \end{Bmatrix}, \quad \{\gamma\}(r) = a\frac{\rho}{8(1-\nu^M)}\begin{Bmatrix} -2(1-2\nu^M) + \rho^2 \\ 2(1-2\nu^M) + \rho^2 \\ 4(1-\rho^2) \end{Bmatrix}$$

and

$$\{\Psi_{ijk}\}(\theta) = \begin{Bmatrix} n_i\delta_{jk} \\ n_j\delta_{ik} + n_k\delta_{ij} \\ n_i n_j n_k \end{Bmatrix}$$

3.4. Interactions with multiple inclusions in the MVE

The perturbed strain in an inclusion is influenced by its interactions with other inclusions in the MVE. In the presence of n_p interacting inclusions, the perturbed strain in an inclusion F_I is written as:

$$\epsilon_{ij}^*(\mathbf{x}^{F_I}) = S_{ijkl}^{F_I}\epsilon_{ij}^{\Lambda_{F_I}} + \sum_{J=1, J\neq I}^{n_p-1} \hat{G}_{ijkl}^{F_J}(\mathbf{x}^I, \mathbf{x}^J)\epsilon_{ij}^{\Lambda_{F_J}} \quad \forall\, \mathbf{x} \in \Omega^{F_I} \tag{41}$$

where the coordinates $\mathbf{x}^I$, $\mathbf{x}^J$ correspond to reference points (e.g. centroids) in the inclusions F_I and F_J respectively. The first term on the RHS is due to self-contribution from the domain Ω^{F_I}, while the second term accounts for interactions with the other $n_p - 1$ inclusions in the ensemble. This equation represents a discrete contribution to the perturbed strain, which can be evaluated only if the configurations and locations of all inclusions are explicitly known. However for large MVE's, only statistical distributions such as the two-point correlation function S_2 in Eq. (17) are known through characterization.

For the population of inclusions represented by a probability distribution function $S_2(\mathbf{r})$ of Eq. (17), the summation in Eq. (41) may be transformed to an integral by using the expected value theorem. The perturbed strain in the fiber F_I $(I = 1\cdots n_p)$ due to the interactions of dispersed fibers in Ω^{mve} can be expressed using Eq. (17) as:

$$\epsilon_{ij}^*(\mathbf{x}^{F_I}) = S_{ijkl}(\mathbf{x}^I)\epsilon_{ij}^{\Lambda}(\mathbf{x}^I) + \int_{\Omega^{mve}\setminus\Omega^{F_I}} S_2(\mathbf{r})\hat{G}_{ijkl}(\mathbf{r})\epsilon_{ij}^{\Lambda}(\mathbf{r})d\Omega \tag{42}$$

where $\mathbf{r} = \mathbf{x} - \mathbf{x}^I$. The second integral term represents the interaction effect of all fibers with the Ith fiber. This approach is termed as the statistically informed Green's function or SIGF in this study.

3.5. Evaluation of eigenstrains

Eigenstrains with n_p interacting inclusions are evaluated by applying Eshelby's stress consistency condition, which requires the total stress inside the fiber Ω^{F_I} be equal to the total stress in the equivalent matrix domain. Using Eq. (26), this is written as:

$$C_{ijkl}^{F_I}\left(\epsilon_{kl}^M + \epsilon_{kl}^*\right) = C_{ijkl}^M\left(\epsilon_{kl}^M + \epsilon_{kl}^* - \epsilon_{kl}^{\Lambda_{F_I}}\right) \quad \forall\, \mathbf{x} \in \Omega^{F_I} \tag{43}$$

where ϵ_{ij}^M is the homogeneous matrix strain. Rearranging the terms, the perturbed strain is written as:

$$\epsilon_{ij}^* + \left(C_{ijpq}^{F_I} - C_{ijpq}^M\right)^{-1}C_{pqkl}^M \quad \forall\, \mathbf{x} \in \Omega^{F_I}\epsilon_{kl}^{\Lambda_{F_I}} = -\epsilon_{ij}^M \tag{44}$$

Substituting Eq. (42) into (44) yields the integral equation for the eigenstrains

$$(M_{ijkl}(\mathbf{x}^I) + S_{ijkl}(\mathbf{x}^I))\epsilon_{ij}^{\Lambda}(\mathbf{x}^I) + \int_{\Omega^{mve}\setminus\Omega^{F_I}} S_2(\mathbf{r})\hat{G}_{ijkl}(\mathbf{r})\epsilon_{ij}^{\Lambda}(\mathbf{r})d\Omega = -\epsilon_{ij}^M \tag{45}$$

where $M_{ijkl}(\mathbf{x}^I) = (C^{F_I}_{ijpq}(\mathbf{x}) - C^M_{ijpq})^{-1}C^M_{pqkl}$.

For a single fiber pair $I-J$, Eq. (45) simplifies to a system of linear equations describing their interaction as:

$$\begin{aligned}
&\left(S^{F_I}_{ijkl} + M_{ijkl}(\mathbf{x}^I)\right)\epsilon^{\Lambda_{F_I}}_{kl} + \hat{\hat{G}}^{F_J}_{ijkl}(\mathbf{r})\epsilon^{\Lambda_{F_J}}_{kl} = -\epsilon^M_{ij} \quad \text{for Fiber } I\\
&\hat{\hat{G}}^{F_I}_{ijkl}(\mathbf{r})\epsilon^{\Lambda_{F_I}}_{kl} + \left(S^{F_J}_{ijkl} + M_{ijkl}(\mathbf{x}^J)\right)\epsilon^{\Lambda_{F_J}}_{kl} = -\epsilon^M_{ij} \quad \text{for Fiber } J
\end{aligned} \tag{46}$$

From these equations, $\epsilon^{\Lambda_{F_J}}_{ij}$ may be eliminated to yield:

$$\begin{aligned}
&\left(S^{F_I}_{ijkl} + M_{ijkl}(\mathbf{x}^I) - \hat{\hat{G}}^{F_J}_{ijmn}(\mathbf{r})\left(S^{F_J}_{mnpq} + M_{mnpq}(\mathbf{x}^J)\right)^{-1}\hat{\hat{G}}^{F_I}_{pqkl}(\mathbf{r})\right)\epsilon^{\Lambda_{F_I}}_{kl}\\
&= \left(\hat{\hat{G}}^{F_J}_{ijmn}(\mathbf{r})\left(S^{F_J}_{mnkl} + M_{mnkl}(\mathbf{x}^J)\right)^{-1} - \tfrac{1}{2}(\delta_{ik}\delta_{jl} + \delta_{il}\delta_{jk})\right)\epsilon^M_{kl}
\end{aligned} \tag{47}$$

where $\mathbf{r} = \mathbf{x}^J - \mathbf{x}^I$.

3.5.1. Eigenstrains for identical fibers

The present analysis assumes that all fibers in the MVE Ω^{mve} have identical shapes and sizes and material properties, and hence:

$$\begin{aligned}
&S^{F_I}_{ijkl} = S^{F_J}_{ijkl} = S_{ijkl}\\
&M_{ijkl}(\mathbf{x}^I) = M_{ijkl}(\mathbf{x}^J) = M_{ijkl}\\
&\hat{\hat{G}}^{F_I}_{ijkl}(\mathbf{r}) = \hat{\hat{G}}^{F_J}_{ijkl}(\mathbf{r}) = \hat{\hat{G}}_{ijkl}(r,\theta)
\end{aligned}$$

where S_{ijkl} and M_{ijkl} are spatially invariant and $\hat{\hat{G}}_{ijkl}$ is position dependent and describes interactions between the fibers. Under these conditions, Eq. (47) is simplified as

$$\begin{aligned}
&((S_{ijkl} + M_{ijkl}) - \hat{\hat{G}}_{ijmn}(\mathbf{r})(S_{mnpq} + M_{mnpq})^{-1}\hat{\hat{G}}_{pqkl}(\mathbf{r}))\epsilon^{\Lambda_{F_I}}_{kl}\\
&= \left(\hat{\hat{G}}_{ijmn}(\mathbf{r})(S_{mnkl} + M_{mnkl})^{-1} - \tfrac{1}{2}(\delta_{ik}\delta_{jl} + \delta_{il}\delta_{jk})\right)\epsilon^M_{kl}
\end{aligned} \tag{48}$$

For the MVE Ω^{mve} consisting of a large number of interacting dispersed fibers, Eq. (48) is represented using an integral term incorporating the correlation function $S_2(\mathbf{r})$. The corresponding eigenstrain ϵ^{Λ}_{ij} in a reference fiber occupying a domain Ω^F is given as:

$$\begin{aligned}
\epsilon^{\Lambda}_{ij}(\mathbf{x}) = &\left[\iota^F(\mathbf{x})(S_{ijab} + M_{ijab}) - \int_{\Omega^{mve}\setminus\Omega_F} S_2(\mathbf{r})\hat{\hat{G}}_{ijmn}(\mathbf{r})(S_{mnpq} + M_{mnpq})^{-1}\hat{\hat{G}}_{pqab}(\mathbf{r})d\Omega\right]^{-1}\\
&\left[\left((S_{abmn} + M_{abmn})^{-1}\int_{\Omega^{mve}\setminus\Omega_F} S_2(\mathbf{r})\hat{\hat{G}}_{mnkl}(\mathbf{r})d\Omega\right) - \frac{1}{2}(\delta_{ak}\delta_{bl} + \delta_{al}\delta_{bk})\right]\epsilon^M_{kl}\\
&= A_{ijkl}(\mathbf{x})\epsilon^M_{kl} \quad \forall\, \mathbf{x} \in \Omega^{mve}
\end{aligned} \tag{49}$$

From Eq. (42), the corresponding perturbed strain at an observation point O (see Fig. 3) is expressed as:

$$\epsilon^*_{ij}(\mathbf{x}) = \left[\iota^F(\mathbf{x})S_{ijmn}(\mathbf{x})A_{mnkl}(\mathbf{x}) + \int_{\Omega^{mve}\setminus\Omega_F} S_2(\mathbf{r}')\hat{\hat{G}}_{ijmn}(\mathbf{r}')A_{mnkl}(\mathbf{r}')d\Omega\right]\epsilon^M_{kl} = B_{ijkl}(\mathbf{x})\epsilon^M_{kl} \tag{50}$$

Here $\mathbf{x}$ and $\mathbf{r}$ are the position vectors of the observation point O and field point J relative to the centroid of a reference inclusion F_I, and $\mathbf{r}' = (\mathbf{x} - \mathbf{r})$. The first-term on the RHS of Eq. (50) exists only when the observation point lies inside the reference fiber, i.e. when $\mathbf{x} \in \Omega^F$ (hence the use of the indicator function). The total strain tensor at a point $\mathbf{x}$ in the presence of the arbitrarily dispersed fibers is then derived to be:

$$\epsilon_{ij}(\mathbf{x}) = \epsilon^M_{kl} + \epsilon^*_{ij}(\mathbf{x}) = \left(\tfrac{1}{2}(\delta_{ik}\delta_{jl} + \delta_{il}\delta_{jk}) + B_{ijkl}(\mathbf{x})\right)\epsilon^M_{kl} = \Xi_{ijkl}(\mathbf{x})\epsilon^M_{kl} \tag{51}$$

where $\Xi_{ijkl}(\mathbf{x})$ is the strain concentration tensor at $\mathbf{x}$ due to the interaction of a fiber with all others in the heterogeneous MVE. The corresponding perturbed displacement at the point $\mathbf{x}$ in the MVE, and on the SERVE boundary Γ^{serve}, is derived by substituting Eq. (49) in Eq. (38) to yield

$$u^*_i(\mathbf{x}) = \left(\int_{\Omega^{mve}\setminus\Omega_F} S_2(\mathbf{r}')L_{imn}(\mathbf{r}')A_{mnkl}(\mathbf{r}')d\Omega\right)\epsilon^M_{kl} \tag{52}$$

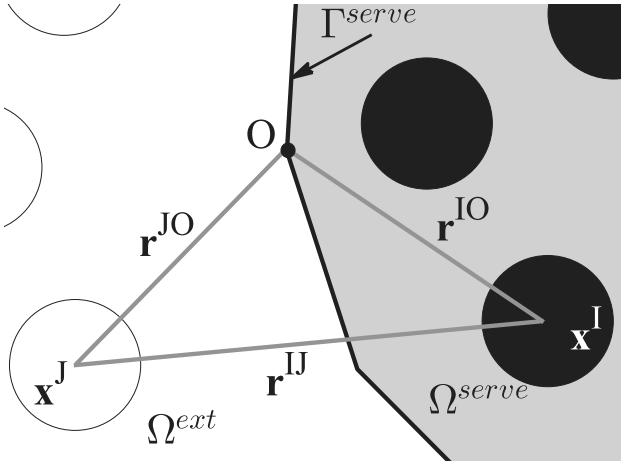

Fig. 3. The effect of an interacting fiber-pair *I* and *J*, in the MVE Ω^{mve} on a field point *O* located on the boundary of the SERVE Γ^{serve}.

Displacement fields on the SERVE boundary Γ^{serve} are therefore represented through the enhancement of the affine transformation based displacements with the perturbed fields in Eq. (52) that account for the exterior statistics-based characterization of the microstructure.

4. Implementation of the exterior statistics-based boundary conditions

The procedure of evaluating and implementing the exterior statistics-based boundary conditions (ESBCs) on the boundary of the SERVE Γ^{serve} is provided in the following steps.

1. Choose the size L of the SERVE domain Ω^{serve} and its corresponding boundary Γ^{serve}. In this study, the cross-section of the chosen SERVE is either a square or an ensemble of Voronoi polygons generated by tessellating the heterogeneous MVE. The SERVE boundary in the latter case is considered to be of two types. The first type corresponds to a periodic boundary that is created by tessellating a domain obtained by periodically repeating the SERVE in the directions of periodicity. The second type corresponds to a boundary that is created by tessellating the domain in its actual morphology.
2. Discretize the SERVE domain Ω^{serve} into a finite element mesh. For the 3D domains considered in this study, 4-noded tetrahedral elements are used.
3. Extract the positions and coordinates (x_j) of all the boundary-nodes on Γ^{serve}.
4. Compute the affine transformation based displacements $u_i^A(\mathbf{x})$ on all the boundary nodes with the applied far-field strain ϵ_{ij}^0 as

$$u_i^A(\mathbf{x}) = \epsilon_{ij}^0 x_j,$$

where x_j is measured relative to the centroid of the SERVE.
5. Compute the two-point correlation function S_2 for the entire MVE domain Ω^{mve} using Eq. (17).
6. Compute the perturbed displacements u_i^* (in a discrete manner) using Eq. (52) with the calculated $S_2(r, \theta)$ in the previous step for all the boundary nodes, extracted in Step 3. The steps followed are:
   - Each radial direction is discretized into N_r number of equally spaced segments with increment $\Delta r = \frac{R-a}{N_r}$, where a is the radius of the fibers, R is the radius of horizon that corresponds to the extent of the MVE. It is important to note that the lower limit of the integration is $r=a$. An αth radial point is given as $r_\alpha = \alpha\frac{R-a}{N_r}$.
   - The angular direction is discretized into N_θ equally spaced points of $\Delta\theta = \frac{2\pi}{N_\theta}$. The βth angular point is given by $\theta_\beta = \beta\frac{2\pi}{N_\theta}$.
   - At a SERVE boundary node at $\mathbf{x}$, the discretized perturbed displacement components in Eq. (52) are evaluated for an applied strain ϵ_{ij}^0 as:

$$u_i^*(\mathbf{x}) = \left[\frac{2\pi(R-a)}{N_r N_\theta}\sum_{\alpha=1}^{N_r}\sum_{\beta=1}^{N_\theta} \alpha L_{imn}(\mathbf{x}-(\alpha\Delta r, \beta\Delta\theta))A_{mnkl}(\mathbf{x}-(\alpha\Delta r, \beta\Delta\theta))S_2(\mathbf{x}-(\alpha\Delta r, \beta\Delta\theta))\right]\epsilon_{ij}^0 \tag{53}$$

7. The exterior statistics-based boundary conditions (ESBCs) on the boundary nodes are computed and applied as:

$$u_i^{ESBC}(\mathbf{x}) = u_i^A(\mathbf{x}) + u_i^*(\mathbf{x})$$

The above procedure is repeated for different SERVE sizes L.

5. Validation tests of the exterior statistics-based boundary conditions (ESBCs)

The validity and effectiveness of applying exterior statistics-based boundary conditions (ESBC) on the SERVE are examined in this section. The SERVE is identified as a statistically equivalent subset of the overall MVE. This section discusses methods for choosing the SERVE from sampling subspaces within the MVE using statistical descriptors. Three-dimensional finite element simulations are conducted, subjected to (i) affine transformation based displacement boundary conditions (ATDBCs), (ii) periodic boundary conditions (PBCs) and (iii) exterior statistics-based boundary conditions (ESBCs). Convergence in the homogenized moduli with increasing SERVE size is taken to be a metric of the effectiveness of boundary conditions.

5.1. Simulations of SERVE with different boundary conditions

To demonstrate the effect of different boundary conditions on the convergence of the SERVE sizes, a MVE is simulated from data generated by microstructural characterization of a unidirectional fiber-reinforced composite in Lenthe and Pollock (2014). The composite is constituted of e-glass-fibers embedded in an epoxy matrix. The image processing tool in MATLAB is used to obtain the centroidal positions and radii of the fibers. The simulated MVE, depicted in Fig. 4, has a section dimension of 1513 μm × 782 μm consisting of 20760 fibers, each having a 4 μm diameter. The average fiber volume-fraction of the entire MVE is $S_1 = 0.2205$. Young's modulus and Poisson's ratio of the epoxy matrix are $E^M = 3.2$ GPa and $\nu^M = 0.4$, while those for the e-glass-fibers are $E^F = 80$ GPa and $\nu^F = 0.25$ respectively.

5.1.1. Microstructural characterization using statistical distribution functions

The fibers in microstructure are of identical size and material properties. Consequently, a maximum of two-point correlation functions i.e. S_1 and S_2 is considered to be adequate in characterizing the two-phase composite (Niezgoda et al., 2008, 2010), as discussed in Section 3.1. To identify SERVEs, sampling subspaces are designated in the microstructural MVE, subsets of which constitute candidate SERVEs. Fig. 4 depicts five highlighted sampling subspaces from SS_I to SS_V belonging to the MVE. The sampling subspaces are chosen from microstructurally distinct regions with non-overlapping boundaries and separated centroids. The subspaces have similar average volume fractions with cross-sections containing 1152 fibers enclosed in squares of ∼ 240 μm. Homogenized stiffness tensor components of the candidate SERVE subsets of these subspaces are used as metrics for establishing convergence criterion for determining the SERVE size.

The correlation functions S_1 and S_2 in the sampling subspaces are evaluated and plotted in Fig. 5. S_1 corresponds to the volume fraction Φ (area-fraction in the case of unidirectional fiber composites) that is defined as the ratio of the fiber volume to the volume of the surrounding matrix. In a dispersed fiber composite, the location dependent S_1 can be obtained by Voronoi tessellation of the microstructure, where the neighborhood of a fiber is represented by its associated Voronoi polygon/polyhedron (Ghosh et al., 1997; Ghosh, 2011). The local area-fraction is then obtained as the ratio of the fiber cross-sectional area to the area of the Voronoi polygon. The probability distribution of S_1 for the MVE with 20760 fibers is shown in Fig. 5(a) (solid-line), while those for the five sampling subspaces are shown with markers. The mode of the distribution, at which the maximum probability density occurs ($\Phi_{mode} = 0.2513$) is different from the mean ($\Phi_{mean} = 0.2205$). This indicates some clustering and matrix-rich regions in the MVE. The distributions of the three sampling subspaces follow the same trend as the MVE. Also the modes of their distribution are very close to 0.2513, indicating that the chosen sampling subspace is statistically similar to the entire sample.

The present analysis assumes statistical isotropy of fiber distribution, i.e. independent of the angular location θ. Hence the two-point correlation function S_2 in Eq. (17) is only dependent on the scalar distance of separation r (Jiao et al., 2007a,b). Fig. 5(b) depicts S_2 as a function of the normalized scalar distance of separation r/a, where $a = 2$ μm is the fiber radius. The S_2 distributions for all the five sampling subspaces, shown with markers, converge to that for the MVE after some initial

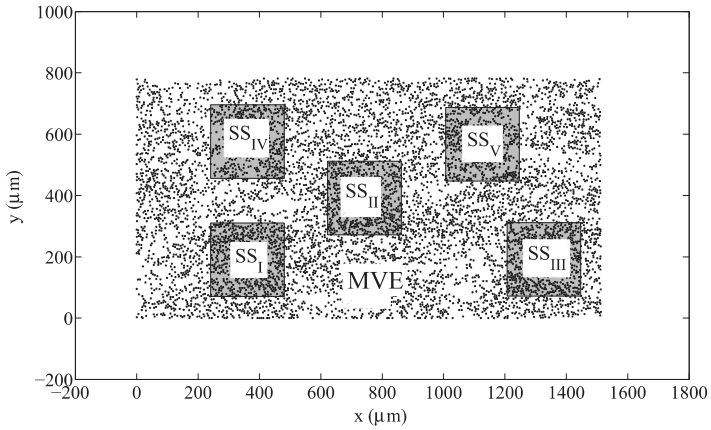

Fig. 4. Microstructural volume element (MVE) of the unidirectional fiber-reinforced composite analyzed, showing a few candidate sampling spaces (SSs).

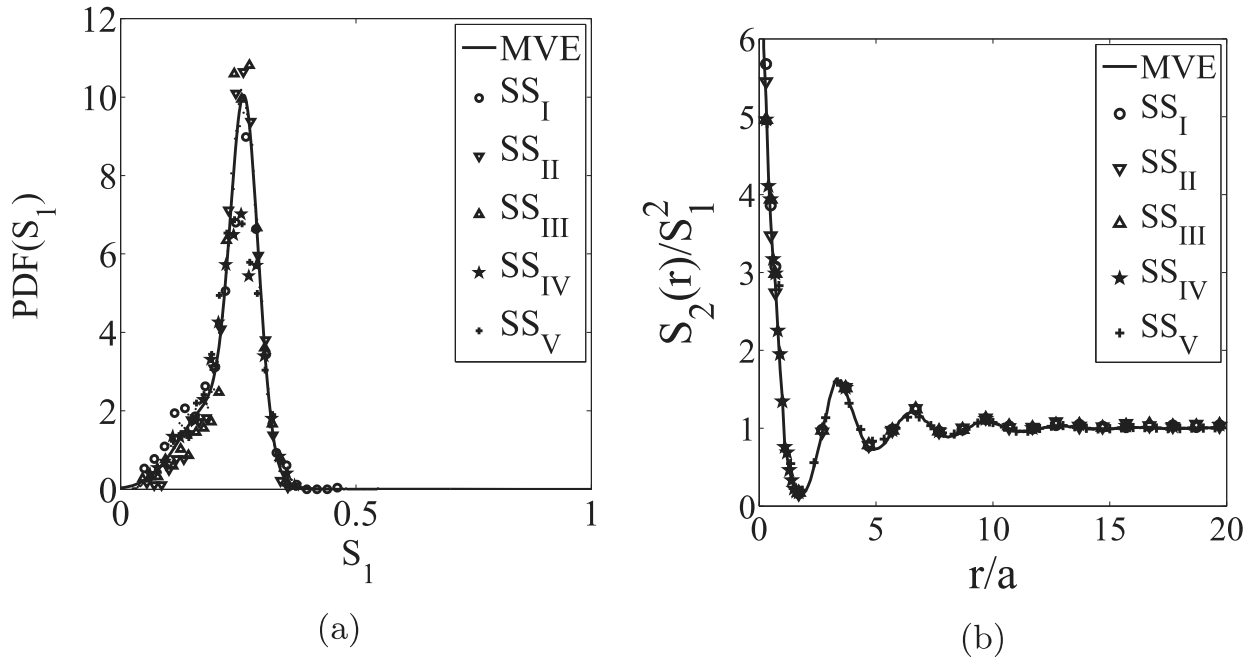

Fig. 5. (a) Probability-distribution of one-point correlation S_1 or local-volume fraction Φ; (b) two-point correlation S_2 as a function of normalized radial distance.

decaying oscillations. As is expected, S_2 tends to Φ^2 for larger distances shown by the dash-dot line. This again demonstrates the statistical equivalence of the sampling subspaces.

Fig. 6 examines the effect of the size of the exterior domain Ω^{ext} ($= \Omega^{mve} \backslash \Omega^{serve}$) on the two-point correlation function S_2, in relation to that of the MVE depicted in Fig. 4. Candidate SERVEs, ranging from 10% to 50% of Ω^{mve}, are excluded from the MVE to establish the domains Ω^{ext}, for which their correlation functions S_2 are calculated. For a SERVE size of $L = 240$ μm that corresponds to the size of the sampling subspace, the exterior domain is ∼90% of the MVE volume. The SERVE size $L = 531$ μm corresponds to an exterior domain that is ∼50% of the MVE volume. The normalized S_2 function for the exterior domains is plotted in Fig. 6 as a function of the normalized distance (r/a). The S_2 function for the MVE is shown as a solid-line, while those for the different exterior domains are shown with markers. In general, the S_2 functions for the different Ω^{ext} show similar variations as the MVE. The difference starts to show only for large SERVEs (smaller Ω^{ext}'s), at larger distances of separation for $r > 15a$. The two-point correlation function of the exterior domains is not significantly affected even when large SERVE volumes are excluded from the MVE. Hence, the two-point correlation functions used in the calculation of the exterior statistics-based boundary conditions (ESBCs) are kept as those for the MVE.

5.2. Accuracy of simulations with exterior statistics-based boundary conditions

The ESBCs for the SERVE, developed using statistically informed Green's function (SIGF) in Section 3, are examined for accuracy. Finite element simulations are performed for the sampling subspace SS_{II} that has a cross-section size of 240 μm × 240 μm, consisting of 1152 dispersed fibers. The first set of simulations corresponds to the applied affine transformation-based displacement boundary condition (ATDBC) u_i^A. Candidate SERVEs are selected from subdomains within SS_{II}. A 40 μm × 40 μm candidate SERVE section, containing 31 fibers is highlighted by the white square boundary in Fig. 7(a). The thickness of the composite domain is taken as 10 μm. It is discretized into a mesh of 4-noded tetrahedral elements having a minimum dimension of 0.8 μm. This corresponds to approximately 13 elements in the z-direction. The ATDBC displacements are $u_i^A = \epsilon_{ij}^0 x_j$, with the applied far-field strain $\epsilon_{11}^0 = 1$. Contour plots of ϵ_{11} are shown on the deformed configuration in Fig. 7 (a). The strain in the fibers is lower than in the matrix due to the larger fiber stiffness.

Displacement solution along the white line is extracted from FE simulations of the SS_{II}. This is compared with the SIGF-augmented solution $u_i = u_i^A + u_i^*$, where u_i^* is the perturbed displacement solution from Eq. (52). The displacement solutions, normalized by the fiber radius, are plotted in Fig. 7(b). The abscissa corresponds to the total length along all sides of the white SERVE boundary. The distance 0–1 corresponds to the bottom edge, 1–2 to the left edge, 2–3 to the top edge and 3–4 to the right edge. Excellent agreement is seen between results of the SS_{II} FE simulations shown with markers, and the SIGF-augmented displacements shown in solid lines. This provides a validation of the ESBC-based SERVE approach. The SIGF-augmented solutions clearly show that even though the far field strain is $\epsilon_{11} = 1$, the u_2 component is not zero on the white SERVE boundary due to fiber interactions. Thus a directly applied ATDBC or PBC on the SERVE boundary will lead to erroneous results.

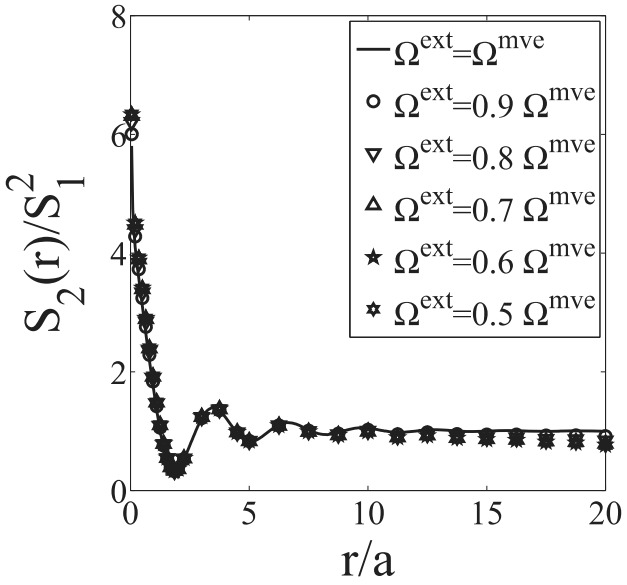

Fig. 6. Two-point correlation (S_2) as a function of the normalized radial distance for the exterior domain Ω^{ext}.

5.3. Candidate SERVE solutions using different boundary conditions

Fig. 8(a) shows a set of seven concentric square cross-sections, corresponding to candidate SERVEs of increasing size and number of fibers, in the sampling subspace SS_{II}. The concentric volumes are chosen to have approximately the same volume fraction as the median volume fraction of the MVE. This is plotted in Fig. 8(b). The solid line corresponds to the median S_1 of the MVE obtained from the probability distribution function in Fig. 5(a), whereas the dots are for the seven candidate SERVEs in Fig. 8(a). The smallest SERVE in Fig. 9(i) consists of 17 fibers in a 35 μm × 35 μm region, and the largest SERVE in Fig. 9 (SS_{II}) contains 1152 fibers in a 240 μm × 240 μm region. Details of the SERVE size and the associated number of fibers are listed in Table 1.

The candidate SERVEs are subjected to ATDBC with $u_i^A = \epsilon_{ij}^0 x_j$, corresponding to a far-field uniaxial strain $\epsilon_{11}^0 = 1$. All other strain components are zero. The corresponding contour plots of the strain ϵ_{11} for the different candidate SERVEs are shown

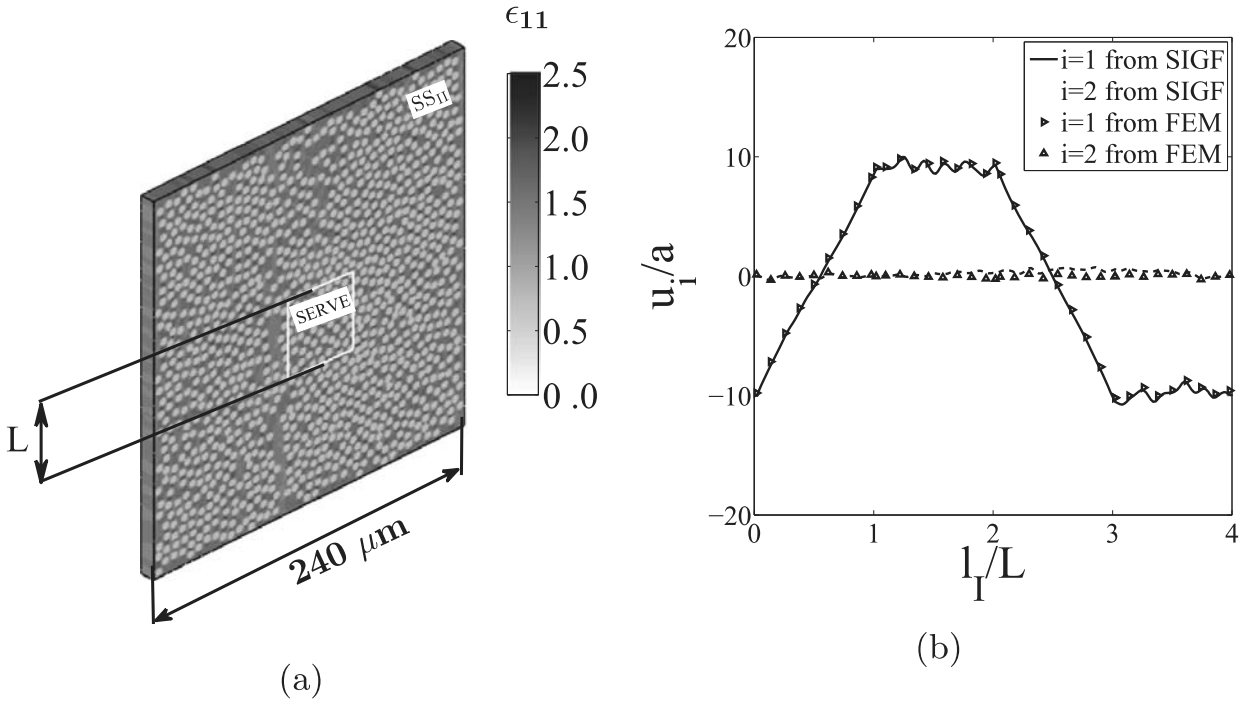

Fig. 7. (a) Contour plot of ϵ_{11} in the sampling subspace SS_{II} subjected to an applied strain $\epsilon_{11}^0 = 1$; (b) comparison of displacements on a candidate SERVE boundary by (i) the exterior statistics-based displacement solution using SIGF and (ii) FE simulations of the region SS_{II}. The abscissa shows the length along the bottom (0–1), right (1–2), top (2–3) and left (3–4) edges in sequence.

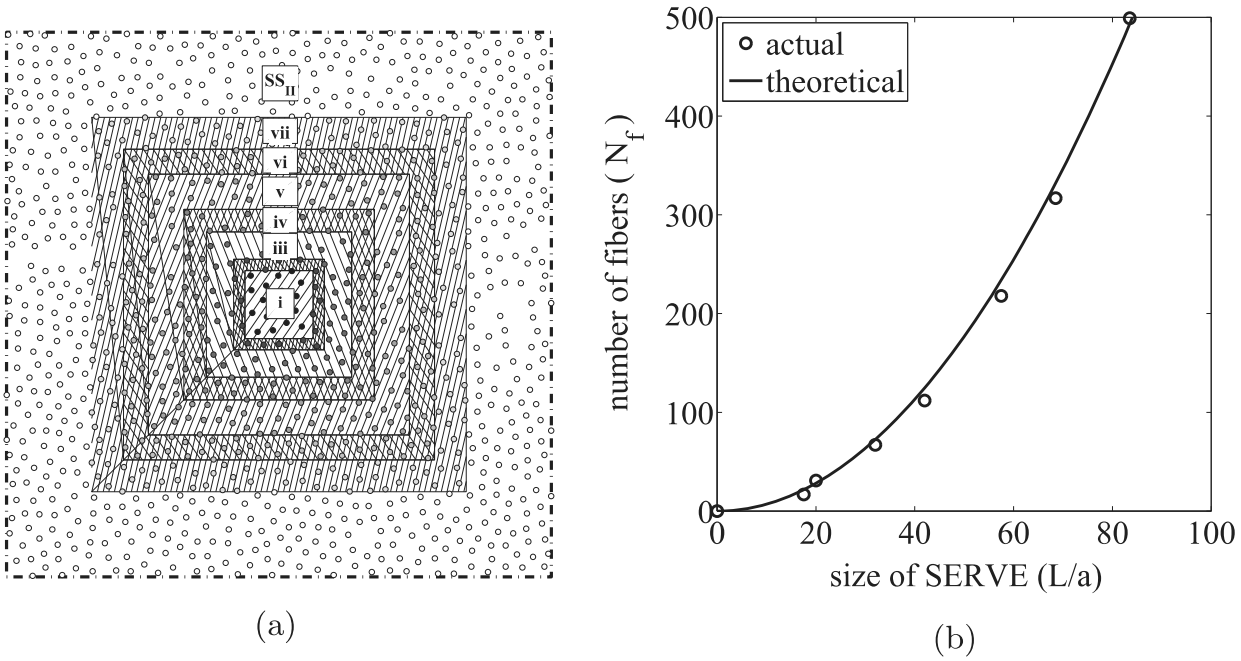

Fig. 8. (a) Concentrically increasing candidate SERVE domains in a sampling subspace SS of the MVE; (b) variation in the number of fibers (N_f) as a function of the SERVE size (L).

in Fig. 9. With ATDBCs, the edges of the SERVE domains remain planar. The strain distribution is non-uniform due to the arbitrary dispersion of fibers. Simulation results obtained by applying ATDBCs and ESBCs on a 40 μm × 40 μm SERVE, containing 31 fibers, are illustrated in Figs. 10 and 11 respectively. The plots in Fig. 10(a) and 11(a) show the displacement components in the 1 and 2 directions along the surface of the SERVE. The abscissa shows the length along the bottom (0–1), right (1–2), top (2–3) and left (3–4) edges of the SERVEs in sequence. The difference between the results with the two boundary conditions is observed in these plots. The perturbations in $u_1 = u_1^A + u_1^*$ with the ESBCs are pronounced on the right and left edges, corresponding to the effect of the exterior domain on the SERVE. While $u_2^A = 0$ for far field strain $\epsilon_{11}^0 = 1$, $u_2 = u_2^*$ is non-zero along the edges with the ESBC. Unlike for PBCs, the deformed edges with the ESBCs are not homologic. Contour plots of the strain ϵ_{11} are depicted in Figs. 10(b) and 11(b). While regions of strain localization are observed in the SERVE with both the boundary conditions, the intensity is found to be less with ESBCs. The contour plot of the difference in the maximum principal stress, obtained by applying the two boundary conditions, is shown in Fig. 12. The difference is

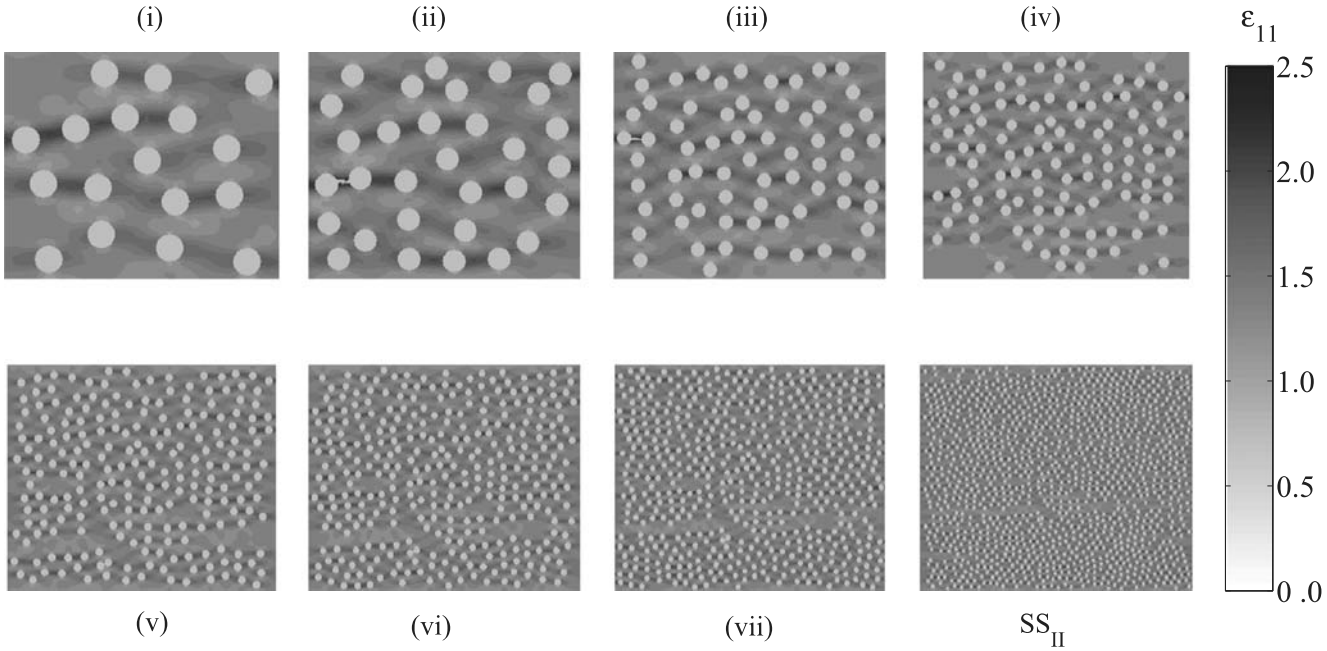

Fig. 9. Increasing square cross-sections of candidate SERVEs in the sampling subspace SS_{II} showing a distribution of the strain ϵ_{11}.

Table 1
SERVE parameters.

SERVE	i	ii	iii	iv	v	vi	vii	SS_{II}
Size L (μm)	35	40	64	84	115	137	165	240
Number of fibers (N_f)	17	31	67	112	218	317	499	1152

pronounced in ligaments between fibers that are in close proximity. The maximum principal stresses are larger with ATDBCs than with ESBCs for the same far-field strains.

Fig. 13 plots the ESBC-based displacement solutions (u_i) for two different SERVE sizes $L = 40$ μm and $L = 165$ μm (ii and vii in Fig. 9), corresponding to a far-field uniaxial strain of $\epsilon^0_{11} = 1$. The displacement components in the ordinate are normalized by the size L to understand the effect of increasing SERVE size on the applied ESBC $u_i = u_i^A + u_i^*$. The perturbed displacements $u_2 = u_2^*$ are higher for SERVE-ii than SERVE-vii in Fig. 13(b). This suggests that the perturbed displacements diminish with increasing SERVE size. Similar results are also seen for u_1.

5.4. SERVE Size from convergence of homogenized stiffnesses

For a continuous undamaged domain Ω, the volume-averaged stresses ($\bar{\sigma}_{ij}$) and strains ($\bar{\epsilon}_{ij}$) are obtained from Eq. (1). The homogenized elastic stiffness tensor components are subsequently calculated from the elasticity relations $\bar{\sigma}_{ij} = \bar{C}_{ijkl}\bar{\epsilon}_{kl}$. Convergence of the homogenized stiffness components with increasing SERVE size is used as a metric to determine the necessary SERVE size. In this study, the dominant stiffness component $\bar{C}_{1111}$ is used for convergence. Details of the procedure for obtaining homogenized moduli have been discussed in Swaminathan et al. (2006a).

To assess the effect of boundary conditions on the converged SERVE size, the homogenized stiffness component $\bar{C}_{1111}$ is plotted as a function of increasing SERVE size L in Fig. 14. The normalized homogenized stiffness from the direct numerical simulation of the entire SS is $\frac{\bar{C}_{1111}}{E^M} = 2.8485$, corresponding to its converged value. In the plot, $L = 0$ corresponds to the matrix alone for which the SERVE size is of zero volume. The different SERVEs considered are shown in Fig. 8(i–vii). An error in the homogenized stiffness component is calculated as the difference between the stiffness components for each SERVE and the entire sampling subspaces in SS_I to SS_V in Fig. 4 with $L = 240$ μm. The plots in Fig. 14(a) show that the homogenized stiffness obtained with the ESBCs converges at a SERVE size of approximately $L = 40$ μm consisting of 32 fibers. In contrast, much larger SERVE sizes of approximately L180 μm are needed when subjected to ATDBCs or PBCs. The error plots in Fig. 14 (b) consolidate this conjecture that convergence with ESBCs is much faster than with the other boundary conditions.This example elucidates the role of exterior statistics on the boundary condition of the SERVE.

The slower convergence of the SERVE when subjected to ATDBCs or PBCs, in comparison to those subjected to ESBCs, is examined further. In Fig. 15(a), two-point correlation functions normalized by the square of the one-point correlation function, i.e. $\frac{S_2}{S_1^2}$, are plotted as a function of the normalized radial distance of separation $\frac{r}{a}$. The $\frac{S_2}{S_1^2}$ values are for the sampling

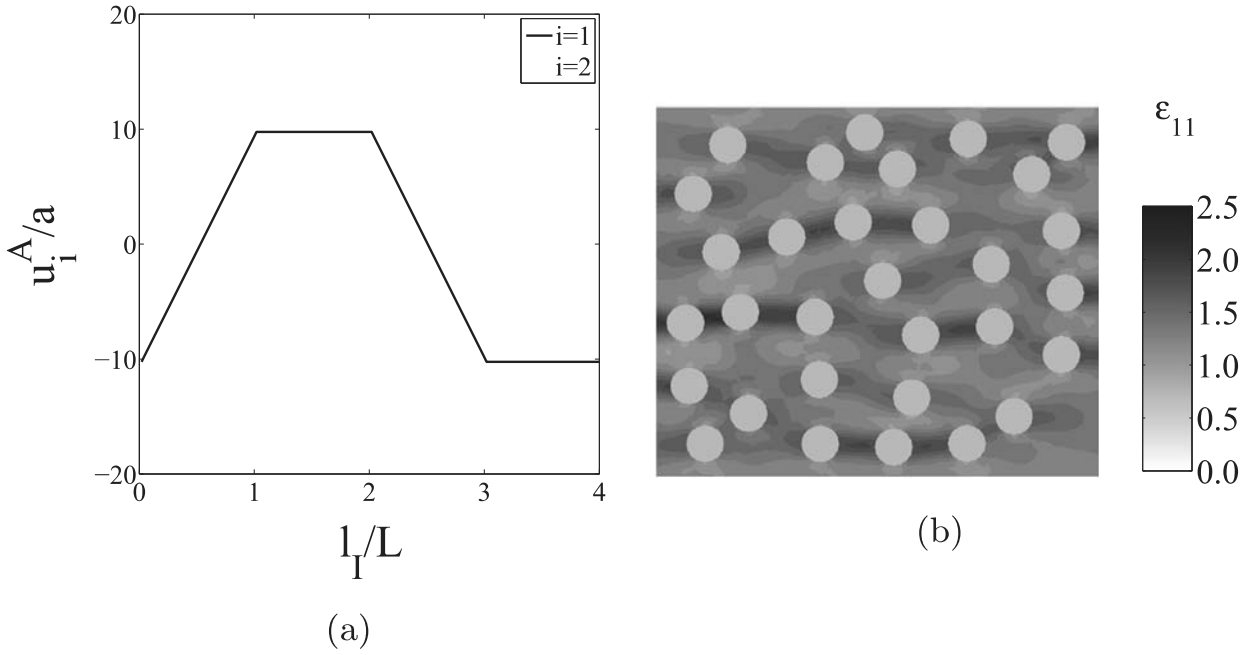

Fig. 10. Results with ATDBCs: (a) displacement along the SERVE boundary (bottom (0–1), right (1–2), top (2–3) and left(3–4)) and (b) contour plot of ϵ_{11} in the SERVE.

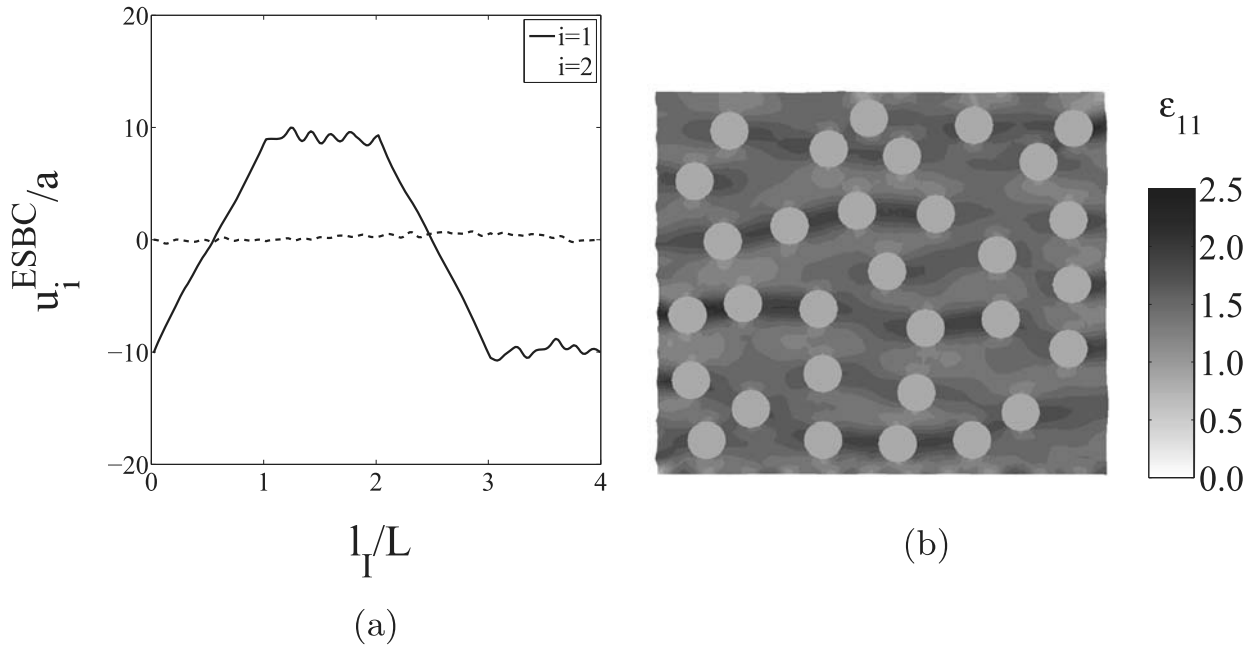

Fig. 11. Results with ESBCs: (a) displacement along the SERVE boundary (bottom (0–1), right (1–2), top (2–3) and left(3–4)) and (b) contour plot of ϵ_{11} in the SERVE.

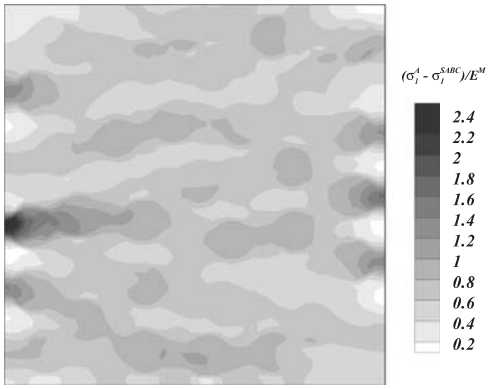

Fig. 12. Contour plot showing the difference in maximum principal stresses in the SERVE by the ATDBCs and ESBCs normalized by the matrix modulus.

subspace SS_{II}, with $L = 240\,\mu m$, as well as for the increasing candidate SERVEs in Fig. 9. As shown in Fig. 5, S_2 for all the sampling subspaces are very similar to that of the entire MVE. The normalized two-point correlation function for all the candidate SERVEs follows the same trend as the MVE, though truncated earlier due to their smaller size. For $r \sim 20a$ corresponding to SERVE sizes $L > 100\,\mu m$ the ratio $\frac{S_2}{S_2^2}$ asymptotically approaches 1. This size $L > 100\,\mu m$, corresponding to $r > 20a$, represents a length-scale beyond which the interactions of between fibers are negligible. This also represents a SERVE size, for which the effect of the fibers in the external domain is minimal. Hence, the convergence of the effective moduli is attained with either ATDBCs or PBCs. This result shows that predictions of the SERVE size from morphology-based characterization functions concur with that from the convergence of effective properties (elastic moduli). For smaller SERVE sizes in the range of $0 < L < 100\,\mu m$ the interaction of fibers in the exterior domain with those in the SERVE is significant and the ESBCs are deemed to be significantly advantageous.

For a more effective measure of the SERVE size, an integral length parameter $\Lambda(R)$ is defined as:

$$\Lambda(R) = \int_0^R S_2(r)dr$$

where R is the largest possible radius belonging to the same phase (inclusions) within a SERVE that is used to evaluate S_2. In general R is dependent on the SERVE size L. Fig. 15(b) plots $\frac{\Lambda(R)}{R}$ as a function of the normalized SERVE size $\frac{L}{a}$. The solid line is a least-square fit of the numerical data for SERVEs in Fig. 8(a), shown with circular markers. As opposed to Fig. 15(a), which depicts an oscillatory convergence, a monotonic convergence to the unit value is seen in this figure with increasing size. Consequently the difference of $\frac{\Lambda(R)}{R}$ from the asymptotic value of 1 may be used as a measure to determine the SERVE size.

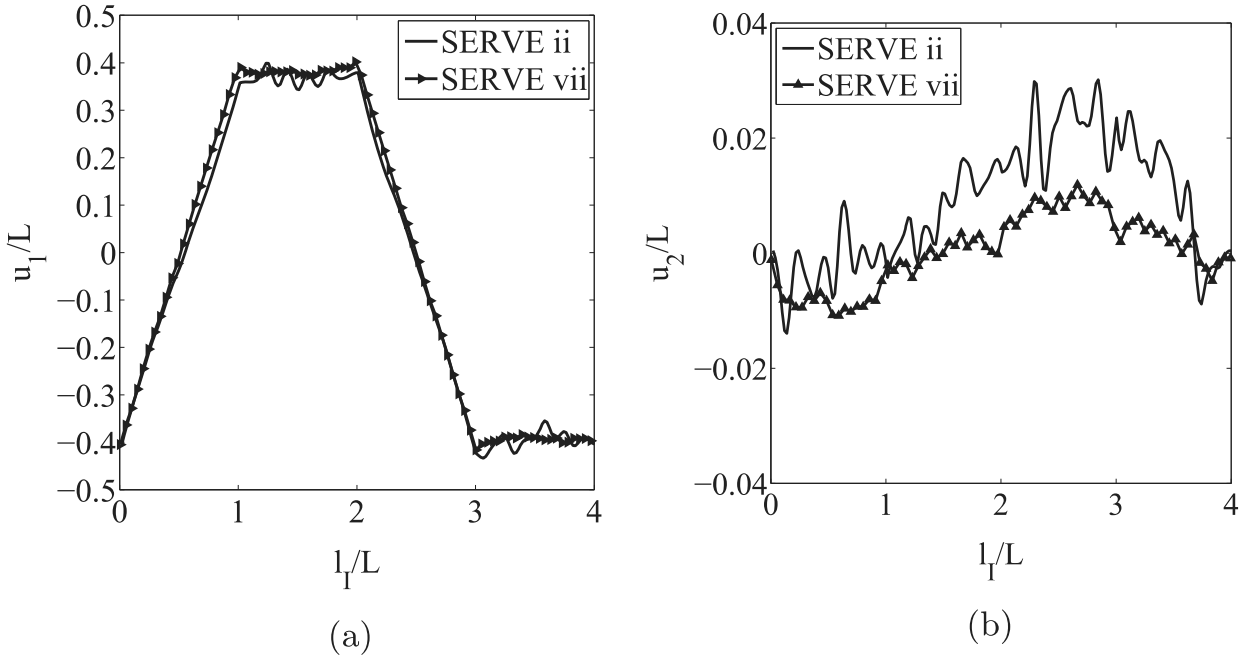

Fig. 13. Effect of the SERVE size on the exterior statistics-based boundary displacement solutions (a) u_1 and (b) u_2 along the boundary.

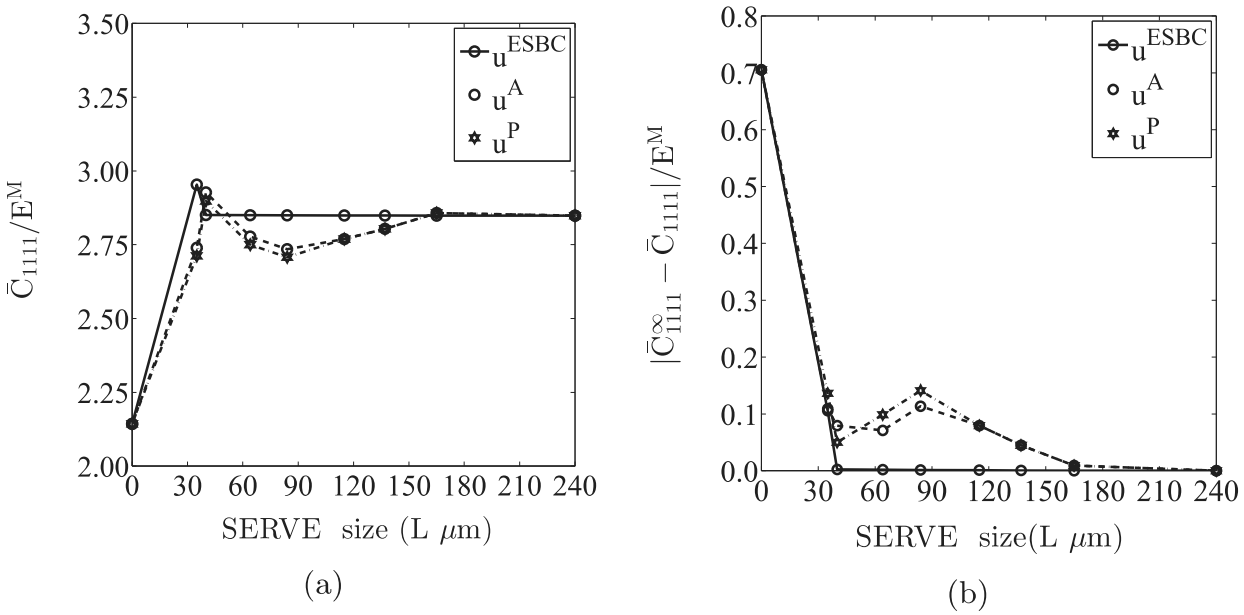

Fig. 14. (a) Variation of the normalized homogenized stiffness tensor $\bar{C}_{1111}/E^M$ and (b) error in $\bar{C}_{1111}$ as a function of the SERVE size.

For example, the SERVE with $L = 115$ μm has a small difference and is hence insensitive to the applied boundary conditions.

6. Comparison of ESBC-based SERVE with statistical and weighted statistical volume elements (SVE/WSVE)

Statistical volume elements (SVE) e.g. in Yin et al. (2008) and McDowell et al. (2011) constitute a designated set of random microstructural volumes, which are too small to satisfy the statistical homogeneity requirements of the RVE for any given response function. In general a large number of SVEs must be simulated to generate the ensemble statistics required to capture the desired responses. The SVE concept is based on the hypothesis that the composite microstructure with dispersed heterogeneities is statistically homogeneous and hence its volume-averages are identical to the ensemble-averages. In the context of this paper, a homogenized modulus obtained for the MVE or a large sampling subspace (SS) is expected to be equal the mean of the volume-averaged modulus obtained from a large number of instantiations of a much smaller analysis volume. This equality in terms of the ensemble-average of any micromechanical variable may be expressed as:

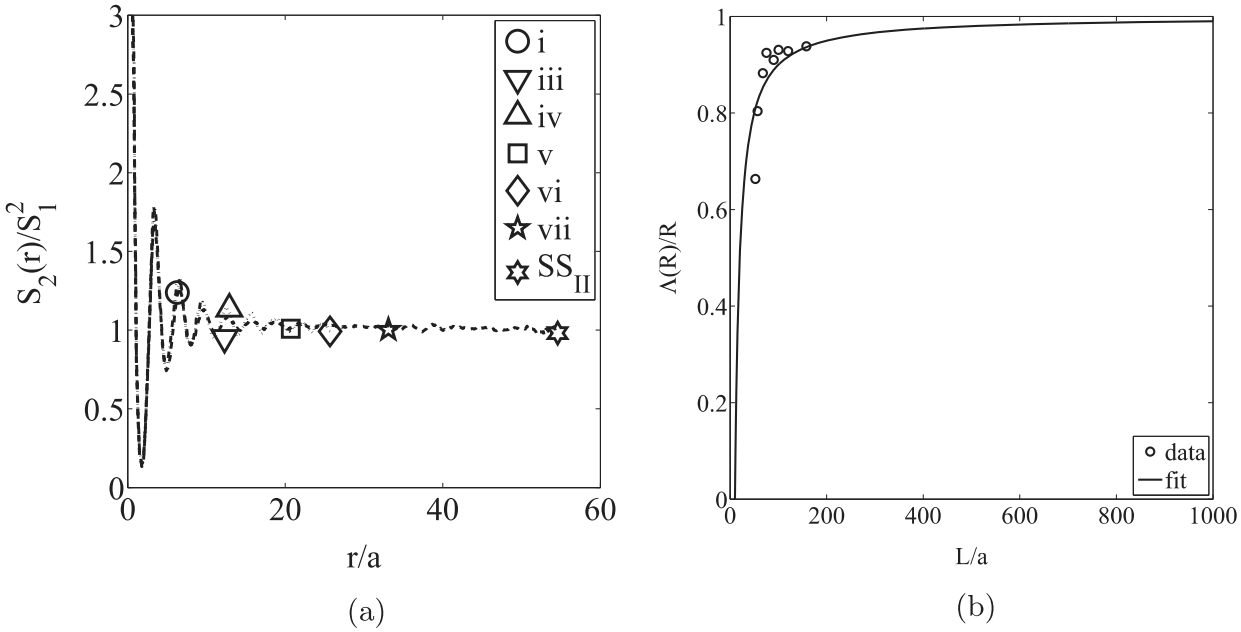

Fig. 15. (a) Two-point correlation functions normalized with the square of the one-point correlation function for the SS_{II} and candidate SERVEs and (b) normalized integral length ($\frac{\Lambda(R)}{R}$) with increasing SERVE size.

$$\bar{\Psi} = \frac{1}{\Omega^{mve}} \int_{\Omega^{mve}} \Psi(\mathbf{x}) d\Omega = \frac{1}{N} \sum_{I=1}^{I=N} \left(\frac{1}{\Omega^{sve_I}} \int_{\Omega^{sve_I}} \Psi(\mathbf{x}) d\Omega \right), \tag{54}$$

where $\bar{\Psi}$ is the volume-averaged value of any spatially varying field quantity $\Psi(\mathbf{x})$, Ω^{sve_I} is the volume of the Ith-instantiation of the SVE and N corresponds to the number of samples in the ensemble. In general, the SVE instantiations follow the size restraint $\Omega^{sve_I} < \Omega^{rve}$.

For comparison with the SERVE predictions, the SVE problem is set up with individual square SVEs of size $L^I = 40\,\mu m$ containing exactly $N_f^I = 32$ fibers. This SVE size is chosen to approximately match the size of the converged SERVE with the ESBCs in Section 5.4, corresponding to a volume-fraction $S_1 = 0.2513$ in Fig. 5(a). A total of 100 candidate SVEs are chosen from the MVE in Fig. 4. The computational SVEs are chosen to be of three forms as shown in Fig. 16, all satisfying the volume fraction constraint. These are:

1. square section with straight-edge boundaries taken from a sampling subspace (SS) domain shown in Fig. 16(a);
2. section with a boundary obtained by Voronoi tessellation of the actual SS to yield SVE domain $\Omega^{sve_I} = \Omega^{SS_{II}} \setminus \Omega^{ext_I}$. This is shown in Fig. 16(b);
3. section that is generated by periodically repeating the core of 32 fibers in the directions of periodicity (x and y) and subsequently performing Voronoi tessellation to generate the SVE boundary (see Ghosh, 2011) as shown in 16(c).

For the periodic microstructures, the boundaries are homologic and can be modeled with PBCs, while for the actual domains with non-homologic boundaries, they can be subjected only to the ATDBCs.

For this study, two-dimensional plane-strain analyses of the 100 candidate SVEs are conducted by prescribing ATDBCs and PBCs separately. A preliminary study is conducted to understand the effect of the boundary geometry and applied boundary conditions on the candidate SVE response. In Fig. 17, strains in the three type of SVEs, subjected to ATDBCs and PBCs are examined, through the contour plots of the axial strain ϵ_{11}. The volume-averaged stiffness components $\bar{C}_{ijkl}$ for a SVE are derived from the relation $\bar{\sigma}_{ij} = \bar{C}_{ijkl}\bar{\epsilon}_{kl}$ between the volume-averaged stresses and strains in Eq. (1). The normalized stiffness component $\bar{C}^I_{1111}/E^M$ for the three types of SVEs with different boundary conditions in Fig. 16 are summarized in Table 2. Since the effects of the boundary geometry or prescribed boundary condition on the stiffness coefficients are not very different, SVEs with square boundaries are considered in the remainder of this study.

In the SVE-based homogenization method, the ensemble-averaged stiffness components $\bar{C}_{ijkl}$ are obtained for the population of N SVEs as:

$$\bar{C}_{ijkl} = \frac{1}{N} \sum_{I=1}^{I=N} \bar{C}^I_{ijkl} \tag{55}$$

where $\bar{C}^I_{ijkl}$ are the volume-averaged stiffness components for the Ith SVE. With increase in the number of instantiations

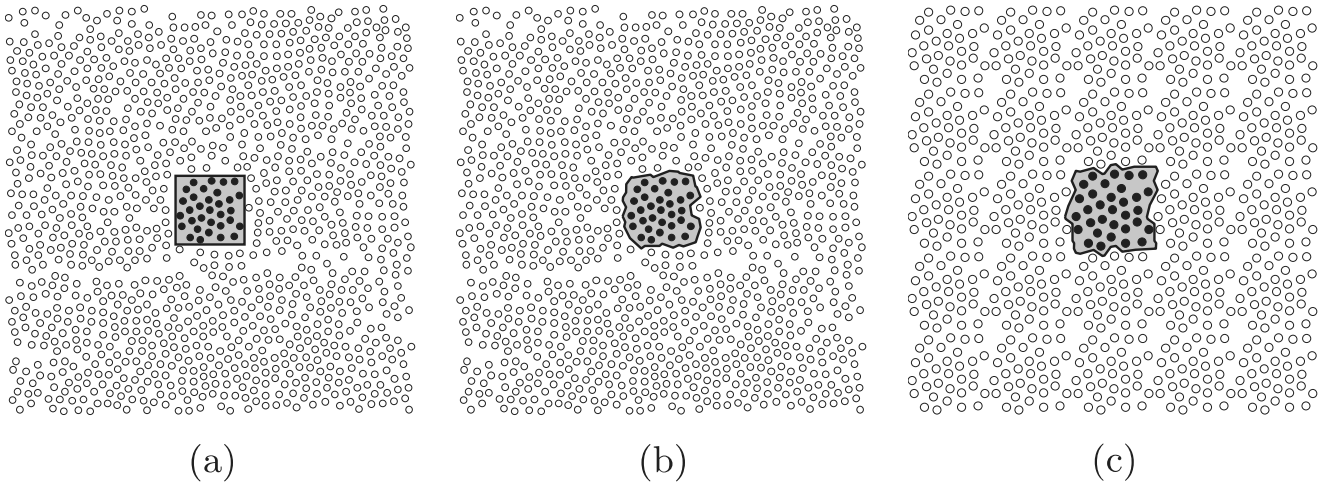

Fig. 16. Different methods of generating boundaries of the statistical volume elements (SVEs): (a) straight-edge boundary square SVE of size 40 μm, (b) boundary generated by Voronoi tessellation of the actual composite domain, and (c) boundary generated by Voronoi tessellation of a region created by periodically repeating a core set of fibers.

corresponding to the ensemble population N, the ensemble averaged stiffness components are expected to converge to their respective homogenized values for the MVE $\bar{C}^{\infty}_{ijkl}$. Convergence criterion is defined in terms of the minimum number of instantiations or SVEs N required in the ensemble to attain a steady-state, invariant value of the homogenized stiffness in Eq. (55). Convergence is ascertained from the plot of the cumulative mean (CM) of the normalized stiffness as a function of the ensemble population size N, as shown in Fig. 18(a). The cumulative mean of a stiffness component $\bar{C}_{ijkl}$ normalized by the matrix Young's modulus E^M is defined as:

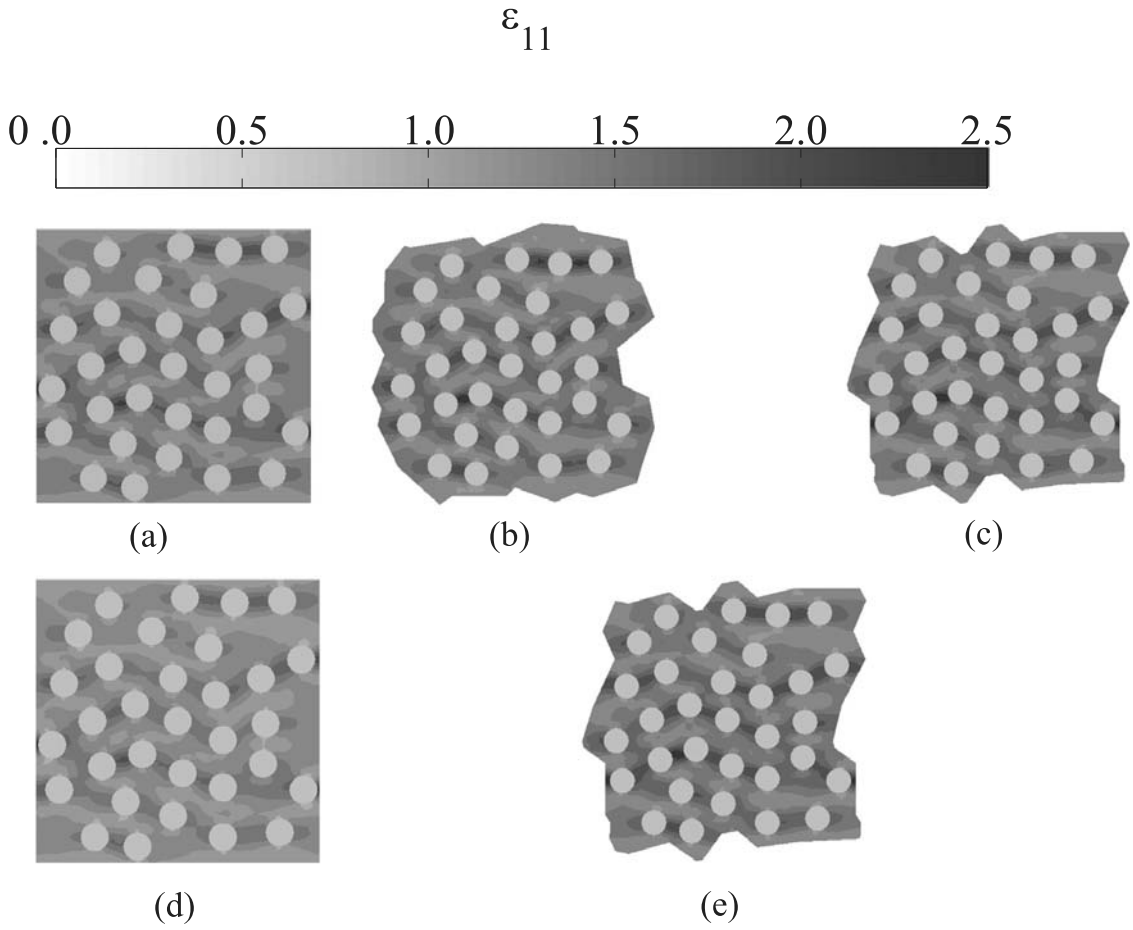

Fig. 17. Contour plots of ϵ_{11} in different types of SVEs with different boundary conditions: ATDBCs on (a) square and (b) actual domain, and (c) periodic domain; and PBCs on (d) square and (e) periodic domain.

Table 2
$\bar{C}^I_{1111}/E^M$ for three types of SVEs under different boundary conditions.

(a)	(b)	(c)	(d)	(e)
2.95	2.96	2.95	2.94	2.94

$$CM\left(\frac{\bar{C}_{ijkl}}{E^M}\right)_N = \frac{1}{NE^M}\sum_{I=1}^{I=N}\bar{C}^I_{ijkl}.$$

For an ergodic microstructure, the cumulative mean of the volume-averaged modulus is expected to converge to that of the entire MVE (or sampling subspaces in this study) $\bar{C}^{\infty}_{1111}$. In Fig. 18(a), the cumulative mean obtained from 100 SVE samples is shown with the dashed line. The SVE size is $L^I = 40$ μm with $N^I_f = 32$. Clearly the stiffness does not converge to $\bar{C}^{\infty}_{1111}$. This lack of convergence indicates that the chosen size of the SVE is inadequate and a larger domain should be considered. On the other hand, the SERVE subjected to the ESBCs converges to $\bar{C}^{\infty}_{1111}$ with only one instantiation of size $L = 40$ μm with $N_f = 32$.

To mitigate convergence limitations of the SVE-based method to the correct stiffness values, a weighted statistical volume element or WSVE-based homogenization method has been proposed in Qidwai et al. (2012). This method uses a weighted ensemble averaging over a number of SVE instantiations. The weighting functions have been obtained from statistical descriptors of the MVE and the candidate SVEs. In the present work, the two-point correlation function S_2 and the integral length parameter Λ are used for determining the weights associated with SVEs. These characterization functions are depicted in Fig. 19.

The maximum, mean and minimum of S_2 and Λ for an ensemble consisting of $N=100$ SVEs are calculated as:

$$\text{mean}(S_2(r)) = \frac{1}{N}\sum_{I=1}^{I=100} S_2^I(r); \quad \text{mean}(\Lambda) = \frac{1}{N}\sum_{I=1}^{I=100}\Lambda^I$$
$$\min(S_2(r)) = \min_{\forall I:(1\le I\le 100)} S_2^I(r); \quad \min(\Lambda) = \min_{\forall I:(1\le I\le 100)}\Lambda^I$$
$$\max(S_2(r)) = \max_{\forall I:(1\le I\le 100)} S_2^I(r); \quad \max(\Lambda) = \max_{\forall I:(1\le I\le 100)}\Lambda^I$$

The variation of S_2 normalized by the square of the volume-fraction, i.e. $\frac{S_2}{S_1^2}$ for the MVE is depicted with a solid line in Fig. 19 (a). For the 100 SVEs, the maximum, mean and minimum values of $\frac{S_2}{S_1^2}$ are also plotted in this figure. The mean value closely follows the variation for the MVE. However the minimum and maximum plots show some scatter. The mean integral length Λ for the 100 SVE instantiations, as well as that for the MVE, is plotted in Fig. 19(b). The difference from the reference MVE values is due to truncation with the smaller volume of the individual SVEs. The weighting functions used in the WSVE approach are calculated as the ratio of the integral length for each SVE to that for the MVE, i.e.

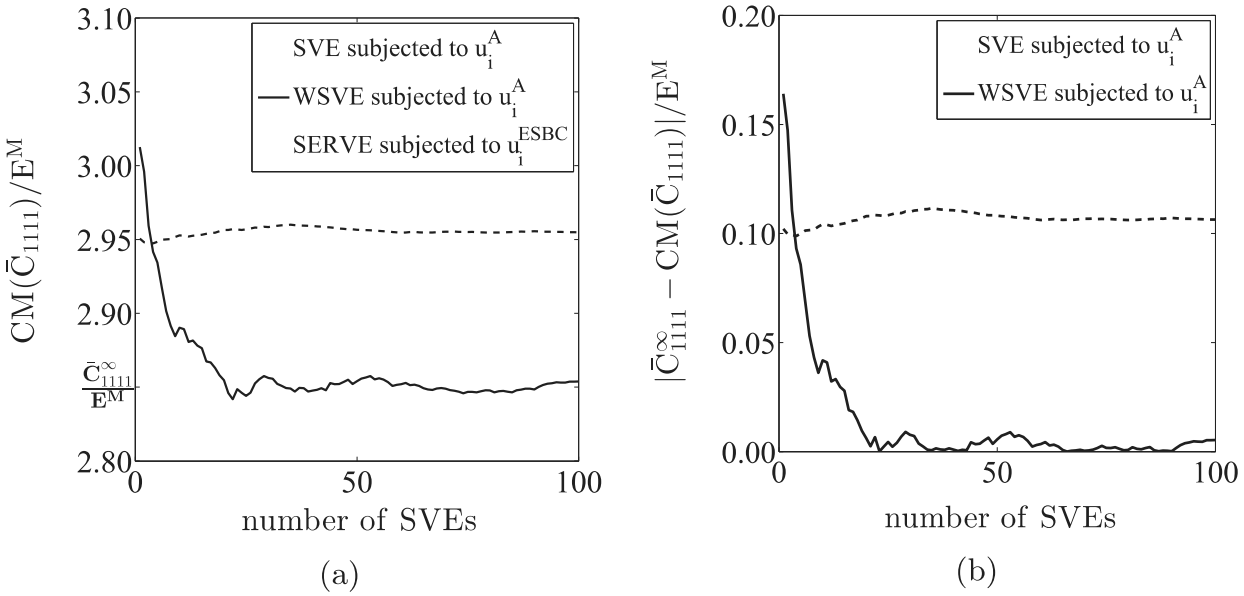

Fig. 18. (a) Cumulative mean (CM) of the ensemble-averaged stiffness as a function of the number of SVEs, by the SVE and WSVE methods; (b) error in CM of the stiffness as a function of the number of SVEs.

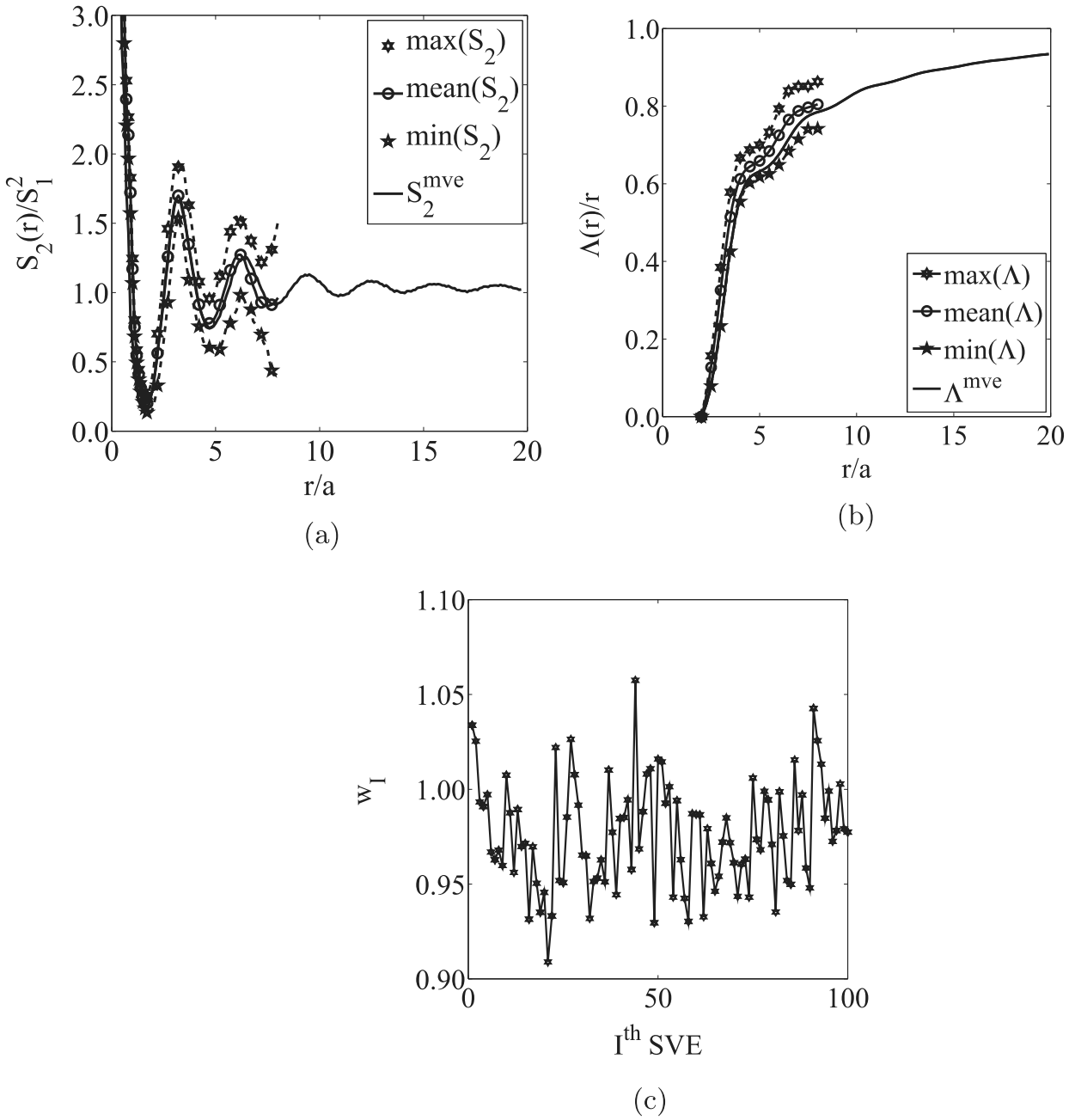

Fig. 19. (a) Plots of normalized two-point correlation function; (b) plot of normalized integral length as a function of normalized radial distance; and (c) plot of weighting functions in the WSVE method as a function of the number of SVEs.

$$w_I = \frac{\Lambda^I}{\Lambda^{mve}}.$$

The weights for the 100 SVEs are plotted in Fig. 19(c).

The weighted cumulative mean of a stiffness component $\bar{C}_{ijkl}$ normalized by the matrix Young's modulus E^M is now defined as:

$$CM\left(\frac{\bar{C}_{ijkl}}{E^M}\right)_N = \frac{1}{NE^M}\sum_{I=1}^{I=N} w_I \bar{C}^I_{ijkl}$$

where w_I are the weights for each SVE instantiation plotted in Fig. 19(c). The weighted cumulative mean converges to the accurate homogenized modulus $\bar{C}^{\infty}_{1111}$ with increasing ensemble population for $N > 20$. While this trend is certainly an advantage over conventional SVEs, the ESBC enhanced SERVE is still significantly more powerful as it converges with a single instantiation. The corresponding error in the cumulative mean, defined as the difference from the stiffness $\bar{C}^{\infty}_{1111}$ of the MVE

(equivalently the sampling subspaces), as a function of the number of SVEs is plotted in Fig. 18(b). The error for the WSVE method progressively decreases with increasing number of SVEs, and tends to be negligible for $N > 20$. However, convergence is not monotonic with the WSVE method due to the oscillations in the weights illustrated in Fig. 19(c).

7. Summary and conclusions

This paper addresses the important problem of defining and identifying the microstructural representative volume element that is commonly simulated to determine response functions and equivalent properties of a heterogeneous material. Statistically equivalent representative volume elements (SERVEs) are needed for microstructures that have nonuniform dispersion of heterogeneities (Swaminathan et al., 2006a,b). Specifically, this paper investigates the role that boundary conditions play on the establishment of the SERVE. Only small deformation elasticity problems are considered in this study. It is known that the conventionally applied uniform displacement, uniform traction or periodic boundary conditions are not optimally accurate representative conditions on these SERVE boundaries. Most of the studies on RVE or SERVE have however ignored the effect of boundary conditions. They determine the extent of the RVE/SERVE domain by analysis with the conventional boundary conditions. This results in a non-optimal RVE domain, often containing a large number of heterogeneities that makes the computational analysis rather tedious.

The major conjecture in this paper is that if boundary conditions imposed are truly representative of the material that is exterior to the SERVE, the SERVE domain required to predict homogenized response functions can be significantly smaller than that with the conventional boundary conditions. A minimum SERVE domain is however required to manifest the necessary deformation mechanisms representative of the microstructure. Thus, if a locally infinite microstructural domain Ω^{mve} is assumed to be constituted of the SERVE domain Ω^{serve} and the complementary exterior domain Ω^{ext}, i.e. $\Omega^{mve} = \Omega^{serve} \cup \Omega^{ext}$, the boundary condition imposed on the SERVE should reflect the interaction between heterogeneities belonging to Ω^{serve} and Ω^{ext}. An additional constraint is that since the exterior domain Ω^{ext} is potentially very large, it is only prudent that a statistical representation of heterogeneities in Ω^{ext} be incorporated in any formulation for deriving the SERVE boundary conditions. This constitutes the objective and problem description for the proposed method.

In this paper, a novel exterior statistics-based boundary condition (ESBC) is developed for the SERVE using statistics of the distributions in Ω^{ext} to build Green's function-based interaction model. This has been termed as the statistically informed Green's function or SIGF approach. The Eshelby equivalent inclusion method is used for manifesting the SIGF-augmented boundary conditions. The advantage of this approach is that the interactions due to the exterior microstructure are represented through the statistical functions rather than individual fibers in the ensemble. The exterior microstructure, for the distributions considered, is adequately characterized by the one-point S_1 and two-point correlation S_2 functions. The effectiveness of the ESBC over other conventional boundary conditions like the affine transformation based displacement boundary condition (ATDBC) and periodic boundary condition is tested through a series of numerical simulations.

The converged size of the SERVE is significantly smaller with the ESBC in comparison with ATDBC or PBC. Next the SERVE subjected to ESBC is compared with other emerging methods like statistical volume element (SVE) and weighted statistical volume element (WSVE). While the ESBC-based SERVE does not need ensemble simulations, the SVE-based methods often require a large number of simulations for convergence. The simulations in this study show that SVEs with a small simulation volume (identical to the SERVE with ESBC) converge to inaccurate values of the macroscopic response function like stiffness. Larger SVE sizes are required for accurate convergence. While this inaccuracy can be rectified in the WSVE approach, large ensemble populations are needed for their convergence.

The proposed method in this paper is deemed as a powerful way of defining the concept of representative volume elements for problems dealing with nonuniform heterogeneous materials. This study is only the beginning of this exploration and future studies will consider strong inhomogeneities such as clustering as well as evolving microstructures with plasticity and damage.

Acknowledgments

This work has been supported through a Grant no. FA9550-12-1-0445 to the Center of Excellence on Integrated Materials Modeling (CEIMM) at Johns Hopkins University awarded by the AFOSR/RSL Computational Mathematics Program (Manager Dr. A. Sayir) and AFRL/RX (Monitors Drs. C. Woodward and C. Przybyla). These sponsorships are gratefully acknowledged. Computing support by the Homewood High Performance Compute Cluster (HHPC) is gratefully acknowledged.

References

Al-Ostaz, A., Diwakar, A., Alzebdeh, K., 2007. Statistical model for characterizing random microstructure of inclusion-matrix composites. J. Mater. Sci. 42, 7016–7030.

Benvensite, Y., 1987. A new approach to the Mori–Tanaka's theory in composite materials. Mech. Mater. 6, 147–157.

Böhm, H.J., 2004. A short introduction to continuum micromechanics. In: Böhm, H.J. (Ed.), Mechanics of Microstructured Materials: CISM Courses and Lectures, vol. 464. . Springer, Wien, NY, pp. 1–40.

Chung, P.W., Tamma, K.K., Namburu, R.R., 2000. A finite element thermo-viscoelastic creep for heterogeneous structures with dissipative correctors. Finite Elem. Anal. Des. 36, 279–313.
Drugan, W., Willis, J., 1996. A micromechanics-based non-local constitutive equation and estimates of representative volume element size for elastic composites. J. Mech. Phys. Solids 44, 1497–1524.
Eshelby, J.D., 1957. The determination of the elastic field of an ellipsoidal inclusion and related problems. Proc. R. Soc. Lond. A241, 376–396.
Feyel, F., Chaboche, J.H., 2000. FE^2 multiscale approach for modelling the elastoviscoplastic behaviour of long fibre SiC/Ti composite materials. Comput. Methods Appl. Mech. Eng. 183, 309–330.
Fish, J., Shek, K., 2000. Multiscale analysis of composite materials and structures. Compos. Sci. Technol. 60, 2547–2556.
Ghosh, S., 2011. Micromechanical Analysis and Multi-scale Modeling using the Voronoi Cell Finite Element Method. CRC Press, Taylor & Francis, Boca Raton, Florida.
Ghosh, S., Lee, K., Moorthy, S., 1995. Multiple scale analysis of heterogeneous elastic structures using homogenization theory and Voronoi cell finite element method. Int. J. Solids Struct. 32, 27–62.
Ghosh, S., Lee, K., Moorthy, S., 1996. Two scale analysis of heterogeneous elastic–plastic materials with asymptotic homogenization and Voronoi cell finite element model. Comput. Methods Appl. Mech. Eng. 132, 63–116.
Ghosh, S., Nowak, Z., Lee, K., 1997. Quantitative characterization and modeling of composite microstructures by Voronoi cells. Acta Mater. 45, 2215–2234.
Guedes, J.M., Kikuchi, N., 1991. Preprocessing and postprocessing for materials based on the homogenization method with adaptive finite element methods. Comput. Methods Appl. Mech. Eng. 83, 143–198.
Hashin, Z., 1983. Analysis of composite materials – a survey. ASME: J. Appl. Mech. 50, 481–505.
Hashin, Z., Shtrikman, S., 1963. A variational approach to the theory of the elastic behaviour of multiphase materials. J. Mech. Phys. Solids 11, 127–140.
Hazanov, S., Huet, C., 1994. Order relationships for boundary conditions effect in heterogeneous bodies smaller than the representative volume. J. Mech. Phys. Solids 42, 1995–2011.
Heinrich, C., Aldridge, M., Wineman, A.S., Kieffer, J., Waas, A.M., Shahwan, K., 2012. The influence of the representative volume element (RVE) size on the homogenized response of cured fiber composites. Modell. Simul. Mater. Sci. Eng., 20.
Hill, R., 1963. Elastic properties of reinforced solids: some theoretical principles. J. Mech. Phys. Solids 11, 357–372.
Hill, R., 1965. A self-consistent mechanics of composite materials. J. Mech. Phys. Solids 13, 213–222.
Hill, R., 1967. The essential structure of constitutive laws for metal composites and polycrystals. J. Mech. Phys. Solids 15, 79–95.
Jiao, Y., Stillinger, F., Torquato, S., 2007a. Modeling heterogeneous materials via two-point correlation functions: basic principles. Phys. Rev. E 76, 031110.
Jiao, Y., Stillinger, F., Torquato, S., 2007b. A superior descriptor of random textures and its predictive capacity. Proc. Natl. Acad. Sci. U.S.A. 106, 17634–17639.
Jones, R., 1975. Mechanics of Composite Materials. Hemisphere Publishing Corporation, USA.
Kanit, T., Forest, S., Galliet, I., Mounoury, V., Jeulin, D., 2003. Determination of the size of the representative volume element for random composites: statistical and numerical approach. Int. J. Solids Struct. 40, 3647–3679.
Kouznetsova, V., Geers, M.G.D., Brekelmans, W.A.M., 2002. Multi-scale constitutive modelling of heterogeneous materials with a gradient-enhanced computational homogenization scheme. Int. J. Numer. Methods Eng. 54, 1235–1260.
Lenthe, W.C., Pollock, T.M., 2014. Characterizing reinforced composite microstructures. Private communication.
Mandel, J., 1971. Plasticite Classique et Viscoplasticite. Springer-Verlag, Udine, Italy.
McDowell, D.L., Ghosh, S., Kalidindi, S.R., 2011. Representation and computational structure–property relations of random media. JOM, TMS 63, 45–51.
Mura, T., 1987. Micromechanics of Defects in Solids, 2nd edition. Kluwer Academic Publishers, Martinus Nijhoff, AA Dordrecht, the Netherlands.
Niezgoda, S., Fullwood, D., Kalidindi, S., 2008. Delineation of the space of 2-point correlations in a composite material system. Acta Mater. 56, 5285–5292.
Niezgoda, S., Turner, D., Fullwood, D., Kalidindi, S., 2010. Optimized structure based representative volume element sets reflecting the ensemble-averaged 2-point statistics. Acta Mater. 58, 4432–4445.
Ostoja-Starzewski, M., 2007. Microstructural Randomness and Scaling in Mechanics of Materials. Chapman and Hall, CRC, Boca Raton, Florida.
Pyrz, R., 1994. Correlation of microstructure variability and local stress-field in 2-phase materials. Mater. Sci. Eng. A – Struct. Mater. Prop. Microstruct. Process. 177, 253–259.
Qidwai, S., Turner, D., Niezgoda, S., Lewis, A., Geltmacher, A., Rowenhorst, D., Kalidindi, S.R., 2012. Estimating the response of polycrystalline materials using sets of weighted statistical volume elements. Acta Mater. 60, 5284–5299.
Romanov, V., Lomov, S., Swolfs, Y., Orlova, S., Gorbatikh, L., Verpoest, I., 2013. Statistical analysis of real and simulated fibre arrangements in unidirectional composites. Compos. Sci. Technol. 87, 126–134.
Shan, Z.H., Gokhale, A.M., 2002. Representative volume element for non-uniform micro-structure. Comput. Mater. Sci. 24, 361–379.
Stroeven, M., Askes, H., Sluys, L.J., 2004. Numerical determination of representative volumes for granular materials. Comput. Methods Appl. Mech. Eng. 193, 3221–3238.
Swaminathan, S., Ghosh, S., Pagano, N., 2006a. Statistically equivalent representative volume elements for unidirectional composite microstructures: part i – without damage. J. Comput. Mater. 40, 583–604.
Swaminathan, S., Pagano, N., Ghosh, S., 2006b. Statistically equivalent representative volume elements for unidirectional composite microstructures: part ii – with interfacial debonding. J. Comput. Mater. 40, 605–621.
Terada, K., Kikuchi, N., 2000. Simulation of the multi-scale convergence in computational homogenization approaches. Int. J. Solids Struct. 37, 2285–2311.
Thomas, M., Boyard, N., Perez, L., Jarny, Y., Delaunay, D., 2008. Representative volume element of anisotropic unidirectional carbon-epoxy composite with high-fibre volume fraction. Compos. Sci. Technol. 68, 3184–3192.
Torquato, S., 1997. Effective stiffness tensor of composite media – i. Exact series expansions. J. Mech. Phys. Solids 45, 1421–1448.
Torquato, S., 2002. Random Heterogeneous Materials; Microstructure and Macroscopic Properties. Springer-Verlag, New York.
Willoughby, N., Parnell, W., Hazel, A., Abrahams, I., 2012. Homogenization methods to approximate the effective response of random fibre-reinforced composites. Int. J. Sol. Struct. 49, 1421–1433.
Yin, X., To, A., McVeigh, C., Liu, W., 2008. Statistical volume element method for predicting microstructure constitutive property relations. Comput. Methods Appl. Mech. Eng. 197, 3516–3529.
Zeman, J., Sejnoha, M., 2007. From random microstructures to representative volume elements. Modell. Simul. Mater. Sci. Eng. 15, S325–S335.
Zohdi, T.I., Wriggers, P., 2004. An Introduction to Computational Micromechanics. Springer, Berlin, Heidelberg, Germany.